MEMORANDUM ON ANALYSIS OF ECHO AREA OF TARGETS USING GEOMETRICAL THEORY OF DIFFRACTION AND CREEPING WAVE THEORY - 2430-1

C. E. Ryan, Jr.

July 1967

DEPUTY FOR SURVEILLANCE AND CONTROL SYSTEMS
ELECTRONIC SYSTEMS DIVISION
AIR FORCE SYSTEMS COMMAND
UNITED STATES AIR FORCE
L. G. Hanscom Field, Bedford, Massachusetts

(Prepared under Contract No. AF 19(628)-67-C-0308 by The Ohio State University, ElectroScience Laboratory, Department of Electrical Engineering, 1320 Kinnear Road, Columbus, Ohio.)

LEGAL NOTICE

When U. S. Government drawings, specifications or other data are used for any purpose other than a definitely related government procurement operation, the government thereby incurs no responsibility nor any obligation whatsoever; and the fact that the government may have formulated, furnished, or in any way supplied the said drawings, specifications, or other data is not to be regarded by implication or otherwise as in any manner licensing the holder or any other person or conveying any rights or permission to manufacture, use, or sell any patented invention that may in any way be related thereto.

OTHER NOTICES

Do not return this copy. Retain or destroy.

ESD-TR-67-519

MEMORANDUM ON ANALYSIS OF ECHO AREA OF TARGETS USING GEOMETRICAL THEORY OF DIFFRACTION AND CREEPING WAVE THEORY - 2430-1

C. E. Ryan, Jr.

July 1967

DEPUTY FOR SURVEILLANCE AND CONTROL SYSTEMS
ELECTRONIC SYSTEMS DIVISION
AIR FORCE SYSTEMS COMMAND
UNITED STATES AIR FORCE
L. G. Hanscom Field, Bedford, Massachusetts

(Prepared under Contract No. AF 19(628)-67-C-0308 by The Ohio State University, ElectroScience Laboratory, Department of Electrical Engineering, 1320 Kinnear Road, Columbus, Ohio.)

FOREWORD

This report, OSURF report number 2430-1, was prepared by The Ohio State University ElectroScience Laboratory, Department of Electrical Engineering, 1320 Kinnear Road, Columbus, Ohio. Research was conducted under Contract F 19628-67-C-0308. Lt. Nyman was the Electronic Systems Division Program Monitor for this research.

This technical report has been reviewed and is approved.

BERNARD J. FILLIATREAULT
Contracting Officer
Space Defense Systems Program Office

ABSTRACT

A combination of creeping-wave analysis and diffraction theory has been developed for determining the radar cross section of bodies for which exact solutions are not available. The known solutions for the perfectly conducting cylinder and sphere have been used to specify attenuation and diffraction coefficients for the creeping wave. The creeping wave contribution is added to the geometrical optics or physical optics contribution from the specular point to determine the total scattered field. It is demonstrated that this type of solution is applicable to ogives, ogives with spherical caps, and prolate spheroids. Wedge diffraction theory has been combined with creeping wave analysis to calculate the edge-on backscatter of circular and ogival disks. It is necessary to modify the magnitudes, but not the forms, of the creeping wave attenuation and diffraction coefficients when treating a creeping wave on an edge. This form of analysis is adaptable to calculation of the radar cross section of composite bodies where both volumetric shapes and edges may occur in combination. Once the specular points, wedge diffraction points, and the attachement points and paths of the creeping waves are determined the computation of the scattered field is straightforward.

TABLE OF CONTENTS

LIST OF SYMBOLS

Electromagnetic fields

U_i	is the incident electromagnetic field,
U_d	is the diffracted field,
E_o, H_o	constants related to the electric and magnetic fields, respectively,
E_r	is the radial electric field on a sphere,
H_ϕ	is the phi component of magnetic field on the sphere
E^i	is the incident electric field,
$u(r, n, \psi)$	a scalar field,
$v(r, n, \phi)$	the total scalar field,
$v^*(r, n, \phi)$	the scalar geometrical optics field,
E_{cw}	the creeping wave component of the electric field,
E_{sp}	the specular point component of the electric field,

Diffraction coefficients

D_i	is the diffraction coefficient at the incidence point,
D_t	is the diffraction coefficient at the point of reradiation,
D^2	$= D_1 * D_t$,
D^2_{og}	is the square of the ogive diffraction coefficient,
D^2_d	the square of the disk diffraction coefficient,

Attenuation coefficients

$\alpha(\rho)$	is the complex attenuation coefficient as a function of local radius of curvature,
α	is a constant attenuation factor,
α_s	is the constant attenuation factor for the sphere,
α_{oc}	is the constant attenuation factor for the cylinder,
α_{og}	is the constant attenuation factor for the ogive,
α_d	is the disk attenuation coefficient,

Co-ordinates, unit vectors, and distances

ρ	is the radius of curvature in the direction of propagation,
ds	is the differential arc length,
L	is the path length along the body,
a	is the radius of a sphere or a semi-axis of a spheroid,
r, R	are distances from the phase reference point,
r_s	is the radius of the spherical cap on the ogive,
ℓ	a distance,

$a = 1+\cos(\phi)$ when used in the limit of an integral,

x, y, z are rectangular coordinates

b is a semi-axis of a spheroid,

$\hat{n}$ the unit normal to a surface,

$\hat{x}, \hat{y}, \hat{z}$ unit vectors of rectangular coordinates,

$\hat{v}$ unit vector in the direction of propagation,

S difference in path length between specular and creeping wave components for the prolate spheroid,

S, L_1, L_2 are distances associated with the ogive and are defined in a figure,

Reflection and transmission coefficients

Υ is a voltage reflection coefficient for the ogive,

$\Gamma = (Z_s - Z_o)/(Z_s + Z_o)$, the reflection coefficient for the spherically capped ogive,

$T_{os} = 2 Z_s/(Z_s + Z_o)$, the transmission coefficient for the spherically capped ogive,

R_w and T_w are reflection and transmission coefficients obtained using wedge diffraction theory,

R_t is the tip reflection coefficient for the ogive,

T_t is the tip transmission coefficient for the ogive,

Impedances

Z_s is the creeping wave impedance of the sphere,

Z_o is the impedance of free space,

Angles

θ_o, θ_1 are angles defined in a figure for spherically capped ogive,

θ, ϕ are angles defined in reference to figures,

θ_{sp} angular location of the specular point,

Miscellaneous

k, k_o $= 2\pi/\lambda$

$F(r_1, r_2)$ is the relative phase function between source and observation points,

λ is the wavelength in free space,

π = circumference of circle/diameter of circle, or

π = 3.1415926535897 approximately

N an integer

τ a dummy variable of integration,

$j = \sqrt{-1}$

σ	the radar cross section,
U1	is a constant related to the diffraction coefficient,
U2	is a constant related to the attenuation coefficient,
R_α	the ratio or the radius of curvature in the direction of propagation of the creeping wave to the orthogonal radius of curvature,
$v_B(r, n, \phi)$	is the Pauli wedge diffraction coefficient,
WA	is the included angle of the wedge
$n = (2\pi - WA)/\pi$	
$G(\theta, \phi)$	is the antenna gain.

MEMORANDUM ON ANALYSIS OF ECHO AREA OF TARGETS USING GEOMETRICAL THEORY OF DIFFRACTION AND CREEPING WAVE THEORY

INTRODUCTION

This report is a preliminary attempt to extend the creeping-wave analysis to bodies for which it has not previously been applied. Several new approaches incorporating geometric diffraction theory and wedge diffraction concepts are proposed and evaluated. This report is intended to summarize the work that has been completed to date and to indicate problem areas which must be investigated in order to develop a consistent creeping-wave theory of scattering. It is not intended to represent a complete analysis of the problem.

The determination of the radar cross section of targets composed of volumetric shapes, ducts, fins, and edges is a difficult but important problem. One approach to this problem is to approximate the target by a collection of shapes for which the individual scattering properties are known and thus estimate the scattered field in a given direction by locating the dominant scatterers and adding their contributions.

A major flaw in this approach is that a general technique for analyzing the part of the body that is in the shadow region or the region not directly illuminated by the incident wave is lacking. Peters[1] showed that a traveling-wave technique is applicable for long thin bodies such as the ogive where the dominant scattering mechanism is chiefly influenced by the part of the body in the shadow region. This technique has been used by all researchers[2] for this type of target despite objections that it lacks mathematical rigor. Franz and Depperman,[3] Keller and Levy[4,5] and others have developed the creeping wave for successfully treating the shadow region of the cylinder. Similar treatment of the sphere has recently been developed.[6] However these solutions are restricted to bodies for which canonical solutions are available. The major purpose of this report is to show that the shadow region of a target can be treated by a relatively simple procedure.

Another approach is the use of point-matching boundary value techniques to generate a system of linear equations which may be solved for the surface currents using a computer. The scattered field is then computed from the surface currents. In this second approach one is limited by the capacity of the computer and the long computation time. This report demonstrates that the techniques of the geometrical theory of diffraction and creeping wave theory offer a means by which the scattering of a composite target can be evaluated to engineering accuracy

using relatively simple formulations which do not require large amounts of computation time. In addition, this analysis allows the evaluation of interactions between the component parts of the scatterer. At the present time only several simple scatterers have been treated. These include the ogive,[1,7] the spherically capped ogive,[8] the finite cone,[10] the cone-sphere,[9] and the disk for edge-on aspects.

The techniques of the geometrical theory of diffraction and creeping-wave analysis depend upon the assumption that the propagation paths of the diffracted and creeping-wave fields may be described using ray tracing and that diffraction is a local phenomenon. These assumptions make it possible to determine the contributing scattering mechanisms of the target for a given direction and also allow the calculation of interactions between parts of the scatterer. The scattered fields are then obtained by summation of the individual contributions.

In order to develop useful diffraction and attenuation coefficients for bodies of revolution, the scattering of the perfectly conducting sphere has been evaluated in the form of a specular point contribution plus a creeping-wave contribution. Physical optics has been assumed to apply to the specular point and the creeping-wave diffraction and attenuation coefficients have been obtained by matching the exact back scattered field at a single value of k_0a. These values were then used to calculate both backscattered and bistatic fields for a range of k_0a values. The excellent result obtained indicated that such a format was useful. This form of solution was then extended to calculate the back scattered fields of a prolate spheroid with good results. The application of this form of solution to the ogive and spherically capped ogive had been done previously[8, 11] and is in agreement with the formulation proposed here.

The impulse technique has also been applied to obtain the scattered fields for the prolate spheroid[12] and for the cone sphere.[9] Basically the impulse solution for the cone sphere is forced to contain the creeping-wave contribution by transforming to the time domain the exact scattered fields for the sphere, after subtraction of the specular scattered fields. The impulse solution for the prolate spheroid makes use of the required behavior in the time domain of the scattered fields to treat the shadow region of the spheroid; i.e., the moment conditions are enforced. This is a clever and rewarding technique which should be pursued further.

In the present report the earlier studies applying the geometrical theory of diffraction technique to these non-canonical shapes are summarized and certain significent points are clarified. In addition certain new mechanisms are introduced.

The wedge diffraction coefficient has been applied to the problem of determining the creeping-wave fields which are transmitted and reflected at a discontinuity of the first derivative of the surface on a body of revolution. Results obtained using this formulation indicate that, to a first approximation, the wedge diffraction coefficient is applicable to bodies of revolution, and thus to three-dimensional scattering in spite of the two-dimensional nature of the wedge scattering problem. The wedge diffraction coefficient has also been applied in combination with creeping waves to determine the scattered fields of a circular disk and a "flat ogive" with excellent results. These results indicate that an extension of these techniques to the analysis of finite edges, such as occur on fins, is practical. Furthermore, the relatively simple form of the equations involved in these computations indicates that this approach could be useful in identifying the geometry in the shadow region.

The creeping wave and diffraction form of analysis permits a simple physical picture of the scattering process. The calculation of the scattered field is straightforward, with the diffraction and attenuation coefficients being simple formulas to evaluate, or program for automatic computation. In general the time required to compute a full 360° back scatter pattern in increments of 2° is less than one minute on an IBM 7094. Thus this technique seems valuable in the determination of radar cross section of complex targets.

New solutions presented in this report include the flat ogive, circular disk for edge-on incidence, the ogive of revolution, and the prolate spheroid.

I. CREEPING WAVE ANALYSIS OF BODIES OF REVOLUTION

A. Review of the Analysis of a Sphere

The concept of creeping waves was introduced by Franz and Depperman[3,13] for the interpretation of the scalar solution for diffraction by a circular cylinder or sphere. Senior and Goodrich[14] have obtained a representation similar to that of Franz and Depperman through the application of the Watson transformation to the Mie series solution for the sphere. Moreland, Peters, and Kilcoyne[8] have applied approximate diffraction and attenuation coefficients developed by Peters[11] to calculate both monostatic and bistatic cross sections of the sphere. Kouyoumjian[15] has also presented a creeping-wave solution for the sphere which includes all higher-order modes. The approach presented here is that of Moreland, Peters, and Kilcoyne.

Referring to Fig. 1 we see that, according to the geometrical theory of diffraction, a portion of the energy incident upon the sphere is trapped at the point of tangency, point A. The ratio of trapped field to incident field is defined as the diffraction coefficient. The trapped energy then travels about the curved body and is attenuated by radiation tangential to the body as it travels. Finally, energy is radiated along a tangent to the body in the scattering direction of interest. The diffraction and attenuation coefficients which describe this process are a function of the radii of curvature of the body in wavelengths. The diffracted field for the lowest-order creeping-wave mode is given by

$$\frac{U_d}{U_i} = D_i D_t \, e^{-j\left[k_o L + \int_A^B \alpha(\rho) ds\right]} \cdot F(r_1, r_2) , \tag{1}$$

where

U_i is the incident field,
U_d is the diffracted field,
D_i is the diffraction coefficient at the incidence point,
D_t is the diffraction coefficient at the point of reradiation,

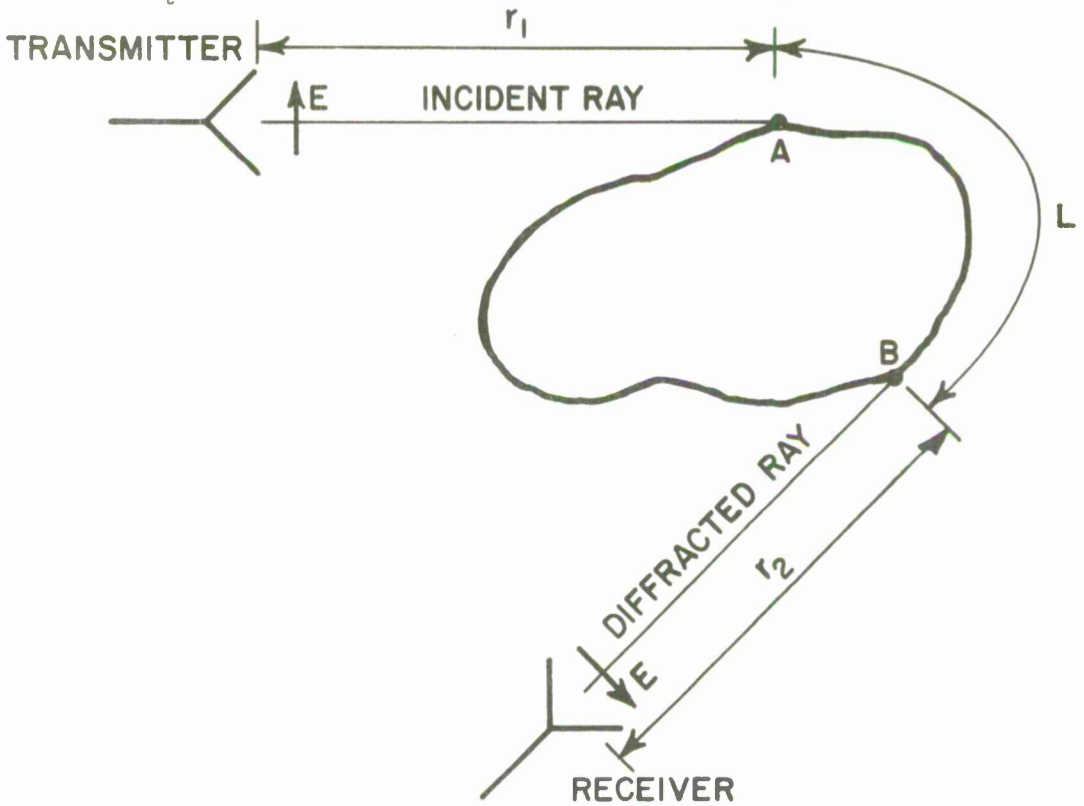

Fig. 1. Scattering by creeping-wave fields.

$\alpha(\rho)$ is the complex attenuation coefficient as a function of local radius of curvature,
ds is the differential arc length,
L is the path length along the body,
k_o is the free space propagation factor, and
$F(r_1, r_2)$ is the phase function relating source and observation points.

If the body has constant curvature, as for the sphere, the radius of curvature at points A and B are equal and the complex attenuation coefficient is constant. Thus Eq. (1) can be written as

$$\frac{U_d}{U_i} = D^2 \, e^{-[\, jk_o L + \alpha L]} \, F(r_1, r_2) \, . \tag{2}$$

Cases for which Eq. (1) must be used are illustrated later as for the prolate and oblate spheroids. In such a case the local radii of curvature at points A and B must be used to evaluate D_i and D_t, and the integral in Eq. (1) must be evaluated.

The diffraction and attenuation coefficients have been derived by comparing solutions in this form to canonical solutions for cylinders, elliptic cylinders, and spheres.[5] This simple description is complicated, however, by the presence of higher-order modes and the existence of higher-order terms in D and α which depend upon the orthogonal radius of curvature.

In the case of the sphere, Keller[16] introduces an additional factor to account for the convergence of rays as they propagate along a geodesic (great circles for the sphere). Keller has evaluated this spreading factor by comparison with the asymptotic form of the exact solution of the scattered fields by the sphere. He finds that the diffraction coefficient and the attenuation coefficient are identical to those for the cylinder. He also introduces a phase jump which results from the caustic formed at the rear of the sphere by the rays propagating along the geodesic. Senior[14] has extended the formulation of the creeping-wave component of the fields scattered by a sphere of small radius by introducing the second term in the asymptotic expansion. His results are in excellent agreement with the exact values, but his analysis cannot be written in a form utilizing diffraction coefficients.

The approach suggested by Moreland, Peters and Kilcoyne,[8] and adopted here, differs from the above in that the exact magnetic fields at the surface of the sphere are used to determine the complex attenuation

coefficient. This approach should include all modes if an accurate approximation to the exact magnetic fields on the surface can be generated. It has been found that throughout the resonance region the attenuation factor for the creeping wave is approximately

$$(3) \qquad \alpha_s = \frac{1}{2}\,\alpha_{oc} = \frac{1}{2}\left[\frac{1}{2a}\,(k_o a)^{\frac{1}{3}}\left(\frac{3\pi}{4}\right)^{\frac{2}{3}} e^{\,j\frac{\pi}{6}}\right] ,$$

where

a is the sphere radius,
k_o is the free space propagation factor, and
α_{oc} is the attenuation factor for the lowest order creeping-wave mode on the cylinder.

The diffraction coefficient, D, has been found by multiplying the diffraction coefficient of the lowest-order creeping wave on the cylinder by a constant. The constant is determined by matching the exact creeping-wave fields on the sphere using the attenuation coefficient given by Eq. (3). The diffraction coefficient is then found to have the form

$$(4) \qquad D_s^2 = 0.27\, a^{\frac{1}{3}} \lambda^{\frac{2}{3}} e^{-j\frac{\pi}{12}} .$$

The process through which these values for the diffraction and attenuation coefficients were obtained is simple and is as follows: The magnetic field shown in Fig. 2 in the shadow region on the surface of the sphere is written as the sum of two creeping waves as

$$(5) \qquad H_\phi = H_o \left[e^{-(jk_o + \alpha_s)\, a\left(\frac{\pi}{2} - \theta\right)} + e^{-(jk_o + \alpha_s)\, a\left(\frac{\pi}{2} + \theta\right)} \right] ;$$

and the radial electric field may be written as

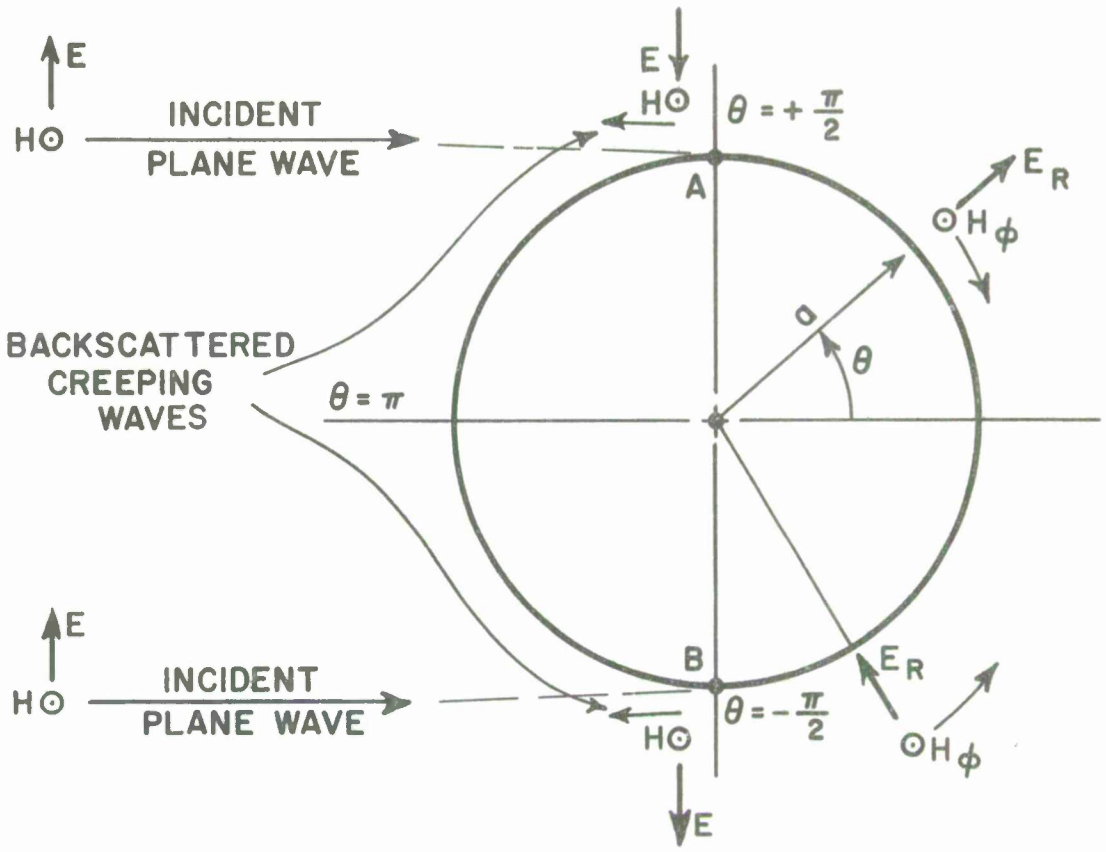

Fig. 2. Creeping waves of the sphere.

$$(6) \qquad E_r = E_o \left[e^{-(jk_o + \alpha_s) a\left(\frac{\pi}{2} - \theta\right)} - e^{-(jk_o + \alpha_s) a\left(\frac{\pi}{2} + \theta\right)} \right] .$$

Now H_o and E_o are chosen to match the exact solution as closely as possible for some value of $k_o a$. A value of $k_o a = 10$ was chosen. Then, assuming α_s to be of the form of α_{oc} one obtains Eq. (3). In slightly abbreviated fashion one may write

$$(7) \qquad \alpha_s = 0.84\, a^{-\frac{2}{3}} \lambda^{-\frac{1}{3}} e^{j\frac{\pi}{6}} .$$

Next, the exact scattered fields are compared to the fields predicted using Eq. (2) and the magnitude of D^2 is determined.

The form of Eqs. (5) and (6) assumes that the creeping waves are launched at points $\theta = \pi/2$ and $\theta = -\pi/2$ and travel in opposite directions

about the sphere. For other attachment points, the paths are parallel to this great circle at the point of attachment. The direction of the creeping waves at the point of attachment is fixed by the Poynting vector of the incident field. After the wave is attached to the surface the minor creeping wave attenuates rapidly, while the major creeping wave is attenuated slowly. Thus the resulting surface wave at some point removed from the shadow boundary has only a radial component of electric field. However the existence of both φ and θ components of the magnetic field at the point of attachment causes a tilt of the Poynting vector on the surface. For points on the shadow boundary removed from the major wave axis this tilt precludes the convergence of rays to form a single caustic at the rear of the sphere.

This approximate form may be compared to the exact solution for the fields on the surface of the sphere along this great circle route through straightforward computation. These fields are illustrated in Fig. 3 for a range of $k_o a$ values. It is seen that fields of the form given in Eqs. (5) and (6) are a reasonable approximation to the exact fields. In addition the backscattered fields due to the creeping wave may be written as

$$(8) \qquad E_{cw} = 2\, D_s^2\, e^{-j2k_o a}\, e^{-(jk_o + \alpha_s)\pi a}\, \frac{e^{-jk_o R}}{R} \quad ,$$

where R is the observation distance from the center of the sphere. The magnitude and phase of the creeping wave obtained using Eq. (8) can be compared to the magnitude and phase of the exact creeping-wave fields obtained by subtracting the specular point contribution of the physical optics term from the exact scattered fields; i.e.,

$$(9) \qquad E_{cw}^{exact} = E^{exact}(k_o a) + \left(1 - \frac{1}{j2k_o a}\right) \quad .$$

where the factor $e^{-jk_o R}/R$ has been suppressed.

The magnitudes of the exact and approximate creeping-wave components are compared in Fig. 4 and their phases are compared in Fig. 5. The agreement is good for a wide range of $k_o a$ values, thus establishing the usefulness of Eq. (8).

The concept of two creeping waves propagating around the sphere may also be used to determine the bistatic scattering in the plane of incidence in a simple manner. Referring to Fig. 6 we see that the components of the bistatic field are

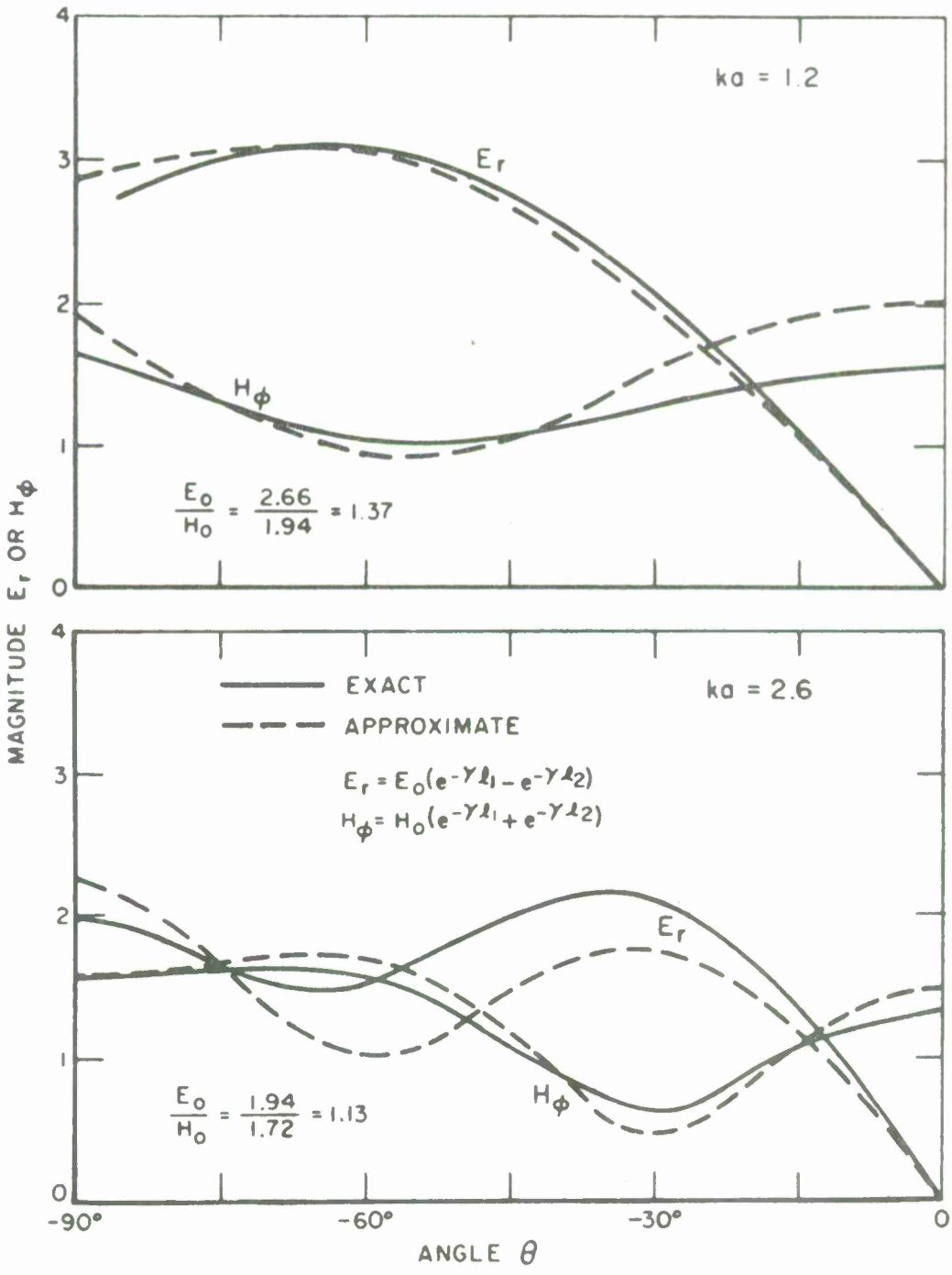

Fig. 3. Normalized fields at the surface of a conducting sphere.

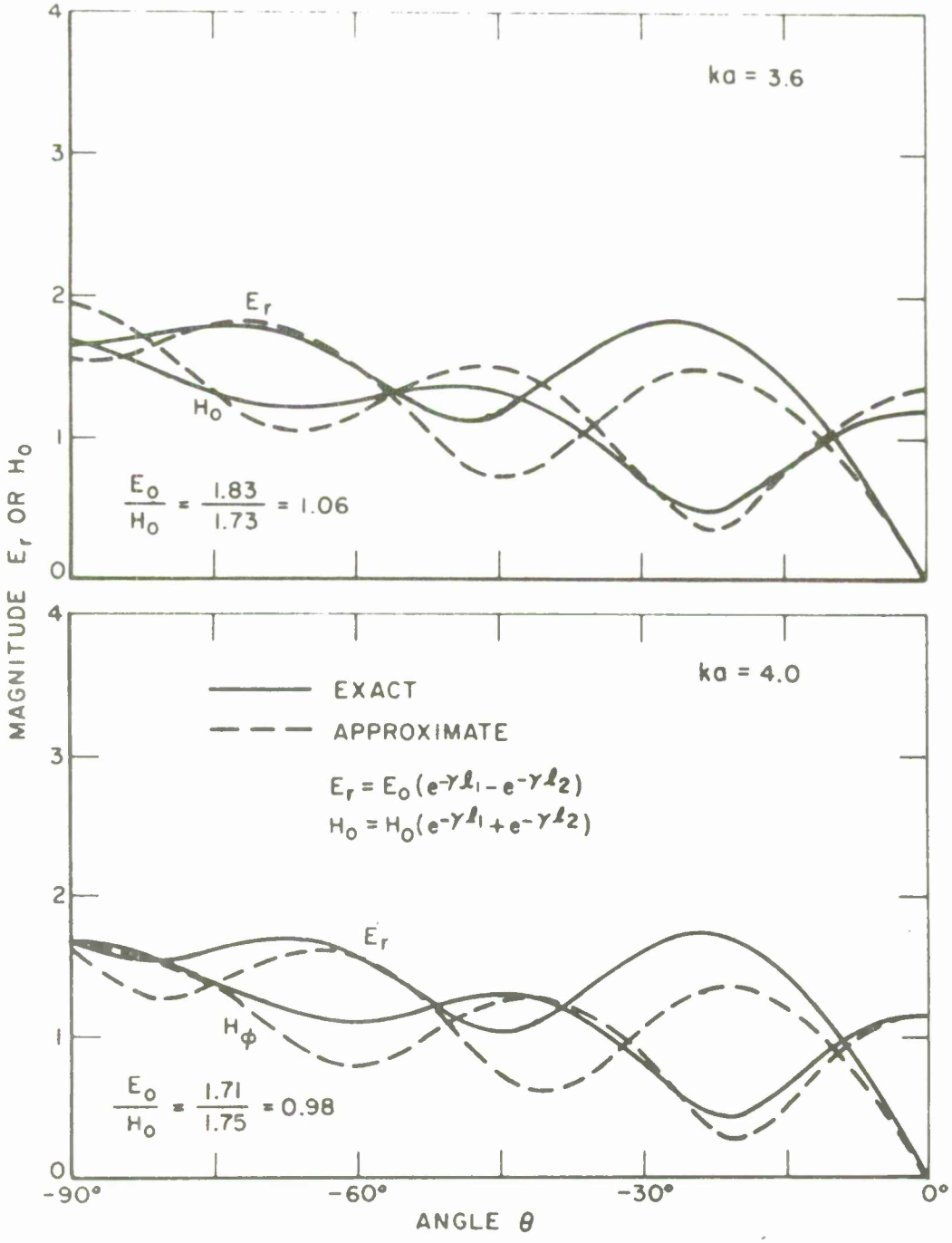

Fig. 3. Normalized fields at the surface of a conducting sphere.

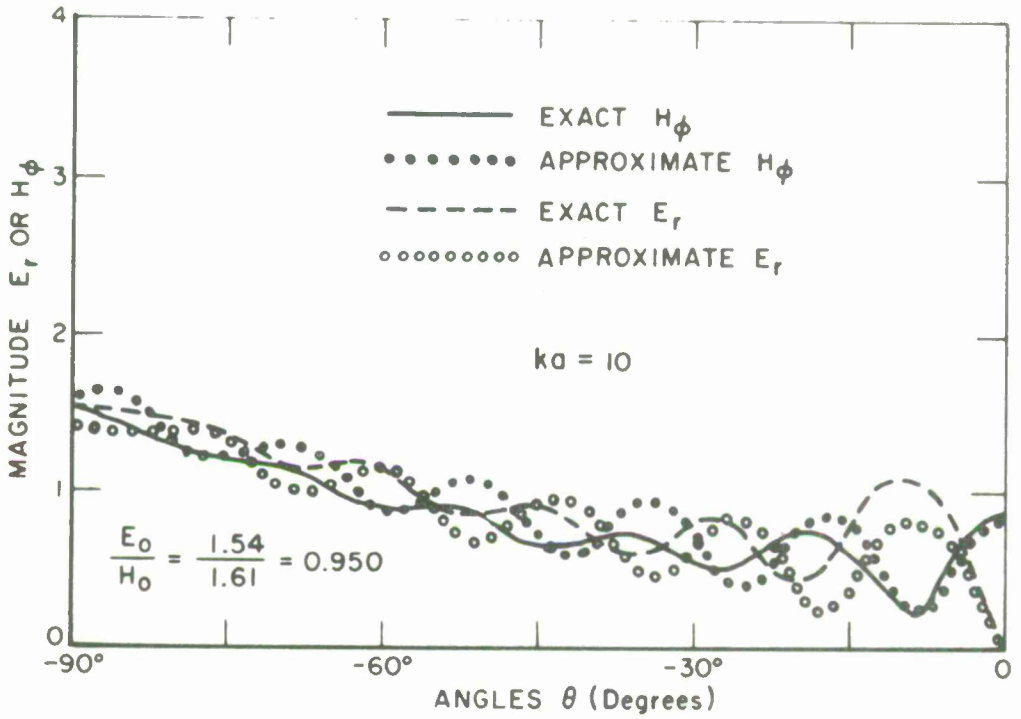

Fig. 3. Normalized fields at the surface of a conducting sphere.

E_{sp}, the specularly reflected field (where it exists);
E_{cw1}, the creeping-wave field reradiated at point A; and
E_{cw2}, the creeping-wave field reradiated at point B.

Thus one may write, the specular term in the form[14]

$$(10) \qquad E_{sp}(\theta) = -\left[1 - \frac{\cos\theta}{j2k_o \cos^3\frac{\theta}{2}}\right] \frac{a}{2R} e^{-jk_oR}$$

and the creeping-wave fields may be written as

$$(11) \qquad E_{cw1} + E_{cw2} = D_s^2 \, e^{-j2k_o\ell}\left[e^{-(jk_o + \alpha_s)\theta a} + e^{-(jk_o + \alpha_s)(2\pi - \theta)a}\right] \frac{e^{-jk_oR}}{R} ,$$

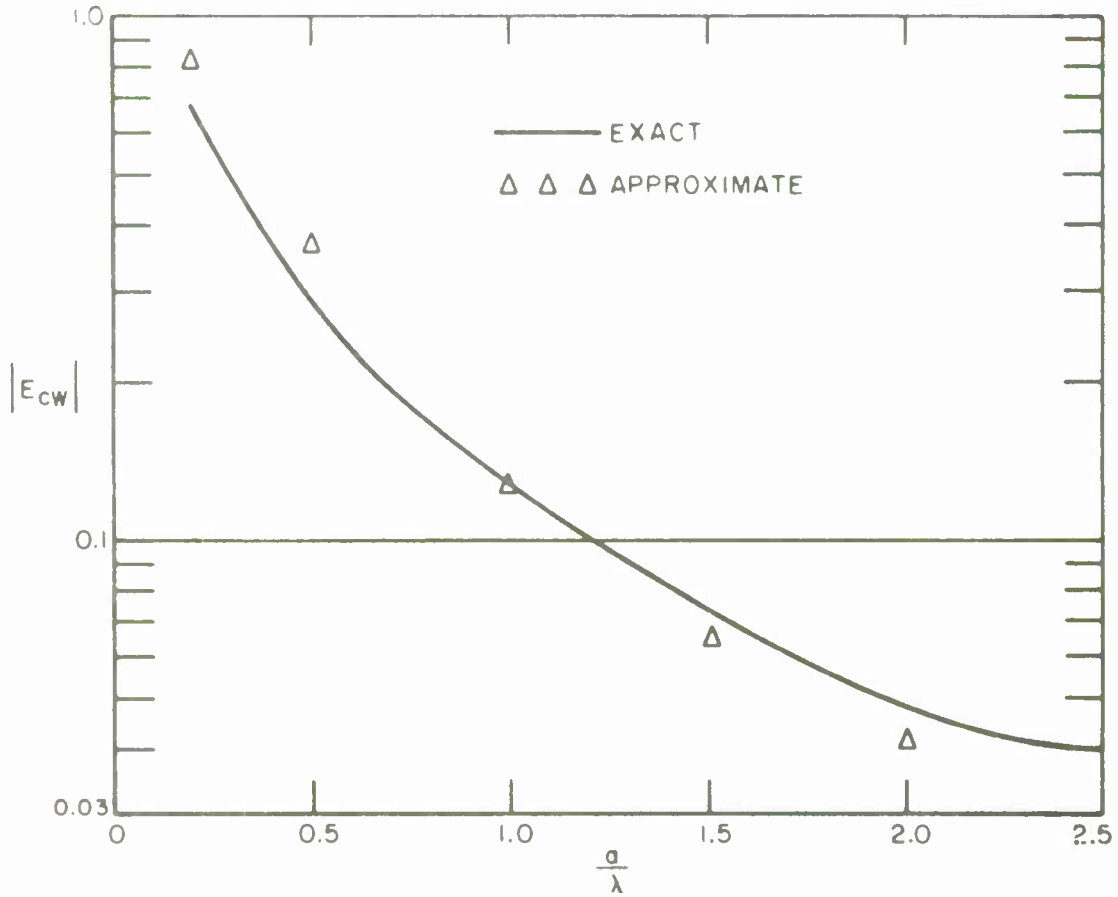

Fig. 4. Absolute relative magnitude of backscattered fields due to creeping waves.

where

$$\ell = a \sin \frac{\theta}{2} \quad .$$

Using the above equations the scattering cross section may be written as

$$(12) \qquad \frac{\sigma}{\pi a^2} = \left| - \left(1 - \frac{\cos \theta}{j2k_o \cos^3 \frac{\theta}{2}} \right) - \frac{2D_s^2}{a} \; e^{-jk_o \ell} \right.$$
$$\left. \left[e^{-(jk_o + \alpha_s)\theta a} + e^{-(jk_o + \alpha_s)(2\pi - \theta)a} \right] \right|^2 \quad .$$

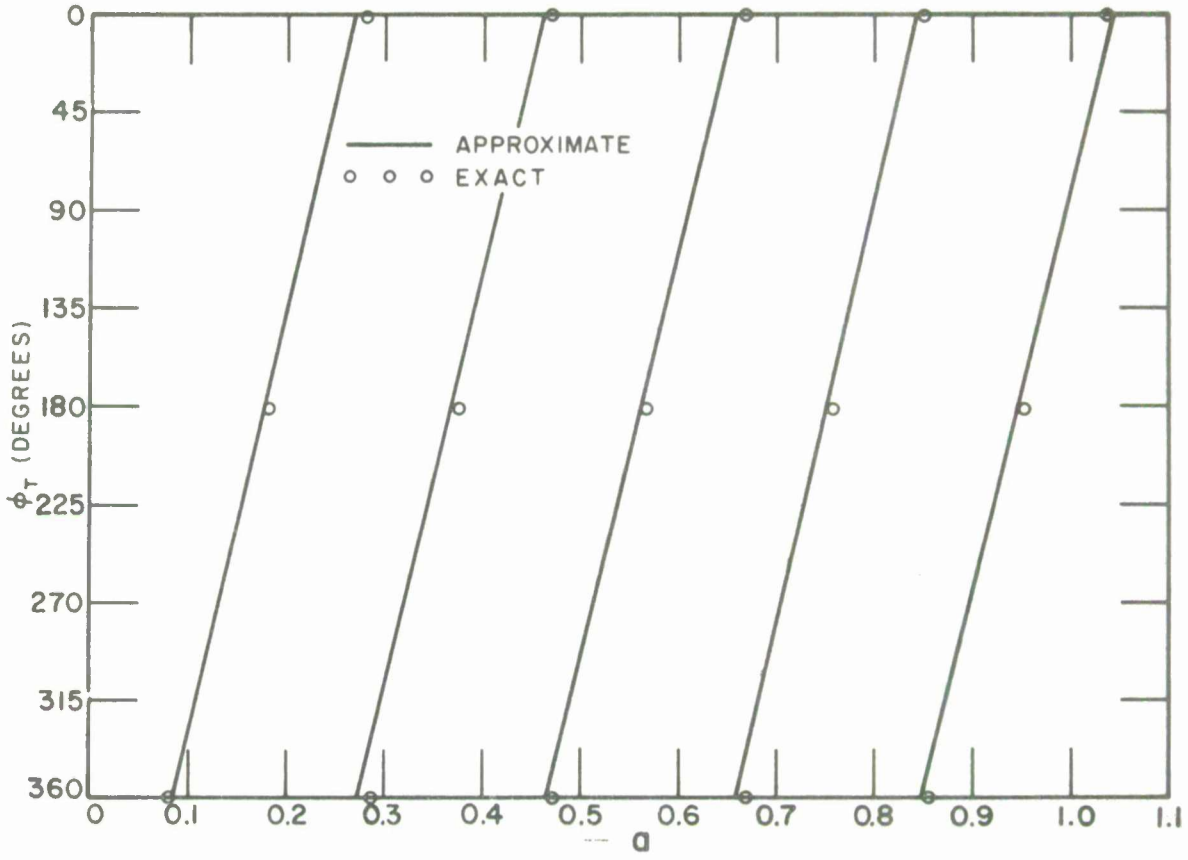

Fig. 5. Phase of backscattered fields due to creeping waves.

A comparison of the approximate bistatic fields calculated using Eqs. (10) and (11) and the exact bistatic fields is presented in Fig. 7.

It is noted that these computations were made by Moreland, Peters, and Kilcoyne.[8] Several computer programs pertaining to both monostatic and bistatic scattering by the sphere are presented in Appendix B. Results obtained using these programs are in agreement with the calculations of Moreland et al.

This form of the creeping-wave solution for the sphere has the advantage of a simple format. The questions of the behavior of the creeping wave fields in the vicinity of the caustic predicted by optics at the back of the sphere are avoided. Also it will be seen that this approach lends itself to a straightforward extension to the analysis of scattering by other bodies of revolution. Furthermore, the consistent results obtained for monostatic and bistatic radar cross section indicate that there is no need to include an integration of the creeping-wave fields about the shadow boundary for the back-scatter case; i.e., to include a

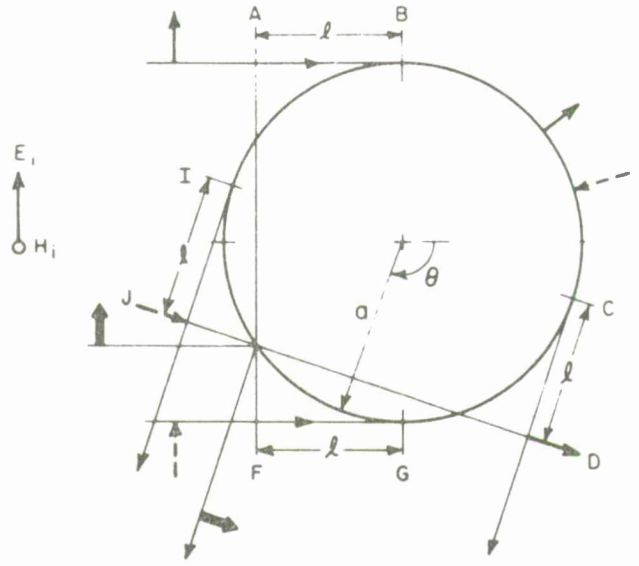

AT BISTATIC ANGLES, θ, THERE ARE THREE FIELD COMPONENTS IN THE RETURN SIGNAL. THEY ARE :

E_{sp}

E_{cw} VIA E_i AT "B"

E_{cw} VIA E_i AT "G"

Fig. 6. Bistatic scattering of the sphere.

glory ray effect. This is consistent with the description of the ray path geometry given previously. The reader should be cautioned, however, that this approach ensures success for the back scatter case in that the effect of caustics, glory rays, etc. can be included in the assignment of values for the diffraction coefficient. For this description to be valid requires that there be no exceptions to it. A contradiction causes the entire explanation to collapse.

B. Analysis of Backscatter by the Prolate Spheroid

The prolate spheroid is similar, with regard to the form of the creeping-wave solution, to the sphere. As in the case of the sphere, the scattered fields are composed of physical optics and creeping-wave contributions. However, for the prolate spheroid, the paths followed by the

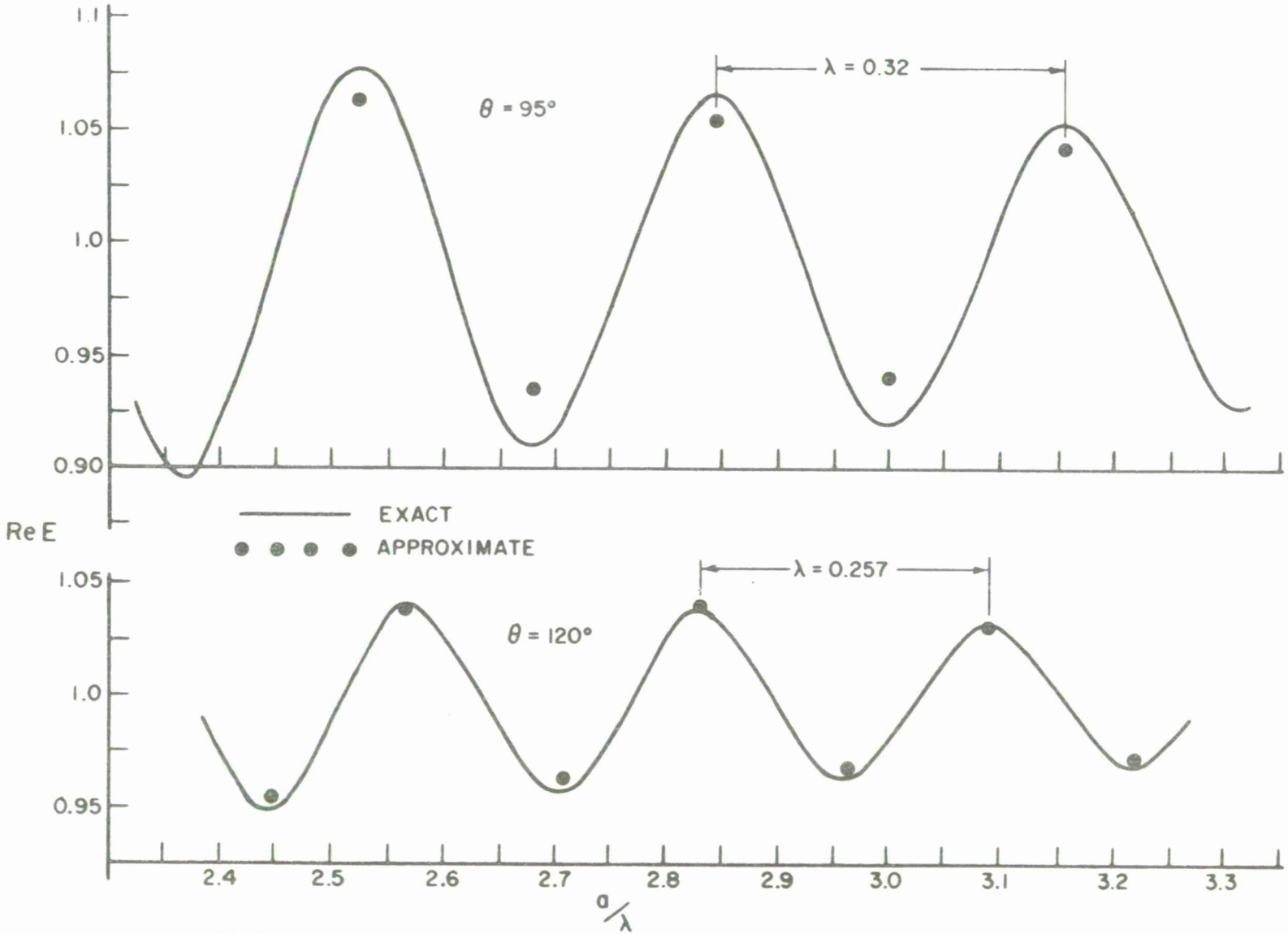

Fig. 7(a). Real part of the bistatic scattered fields of the sphere.

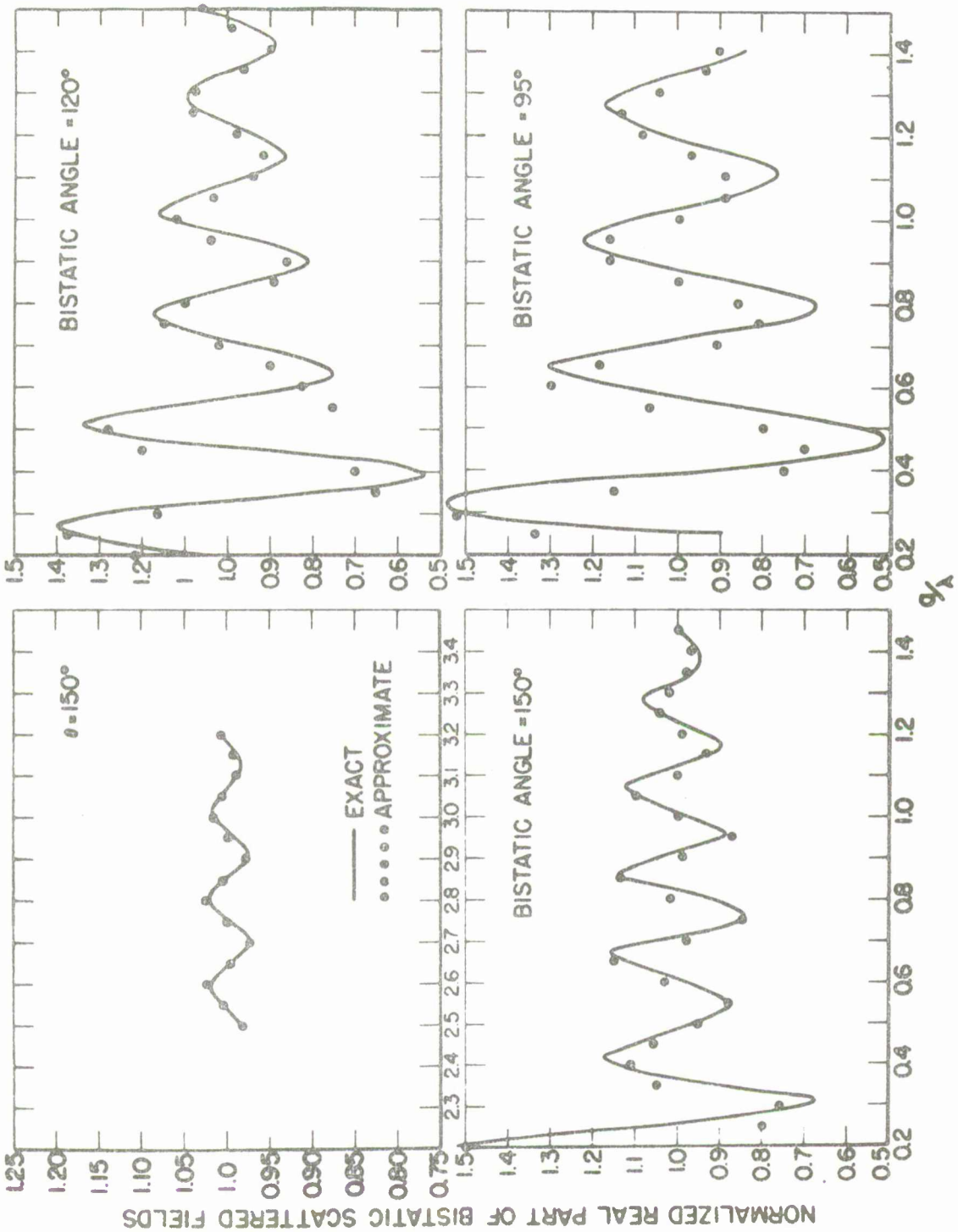

Fig. 7(b). Real part of the bistatic scattered fields of the sphere.

creeping waves on the body are, in general, ellipses. Thus the radius of curvature in the direction of propagation is continually changing and it is necessary to compute the integral in Eq. (1). The coordinate system used for the prolate spheroid is shown in Fig . 8.

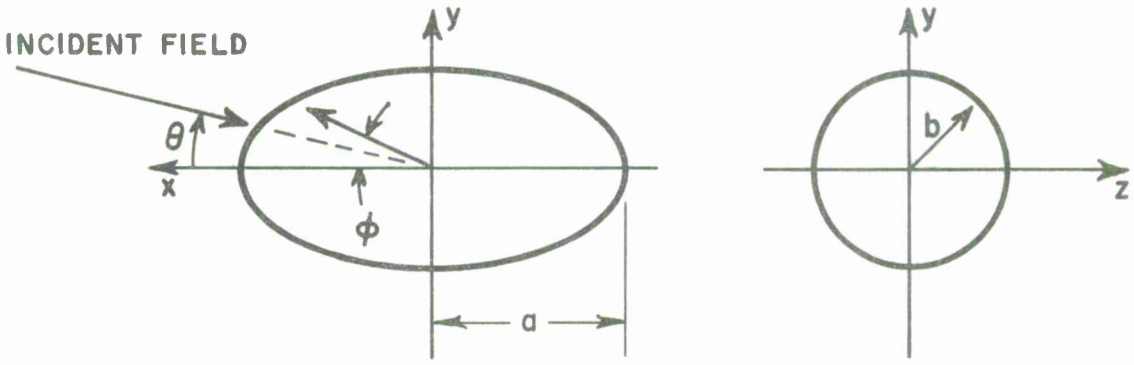

$$\frac{x^2}{a^2} + \frac{y^2+z^2}{b^2} = 1$$

Fig. 8. Coordinates for the prolate spheroid.

The prolate spheroid has previously been studied by Moffatt[12] using time domain analysis. Moffatt's approach is similar to the creeping-wave approach in that he approximates the impulse response through the use of a "physical optics" contribution in the form of an impulse at time t = 0, which decays and joins into a creeping-wave return at time t = T_o (where T_o corresponds to the time required for the creeping wave to propagate around the spheroid). The form of the impulse response postulated by Moffatt is shown in Fig. 9.

Following this line of reasoning and referring to Fig. 10 we may write the back scattered creeping-wave field for a wave incident in the x-y plane, with polarization lying in the x-y plane, as

$$E_{cw} = 2\, D^2\, e^{-jk_o L}\, e^{-\int_A^B \alpha(\rho)ds} \quad , \tag{13}$$

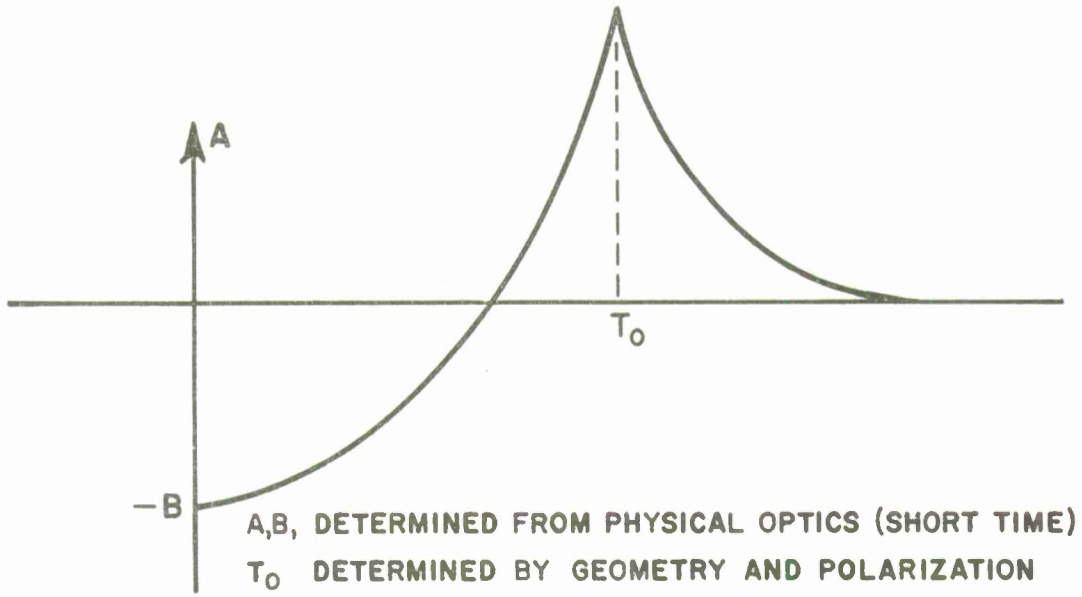

Fig. 9. Impulse response of the prolate spheroid.

where

$$L = \int_A^B ds$$

and

ds = differential arc length.

A similar expression may be written for arbitrary incidence direction and polarization, as illustrated in Fig. 11, but we shall examine the simplest case. For the case illustrated in Fig. 10 (parallel polarization) we may write the radius of curvature in the incidence plane containing the E vector as

$$\rho = (a^2 \sin^2 \phi + b^2 \cos^2 \phi)^{3/2} / ab \,, \tag{14}$$

which is readily derivable from the parametric form of the equation of the ellipse. Likewise the differential element of arc length is

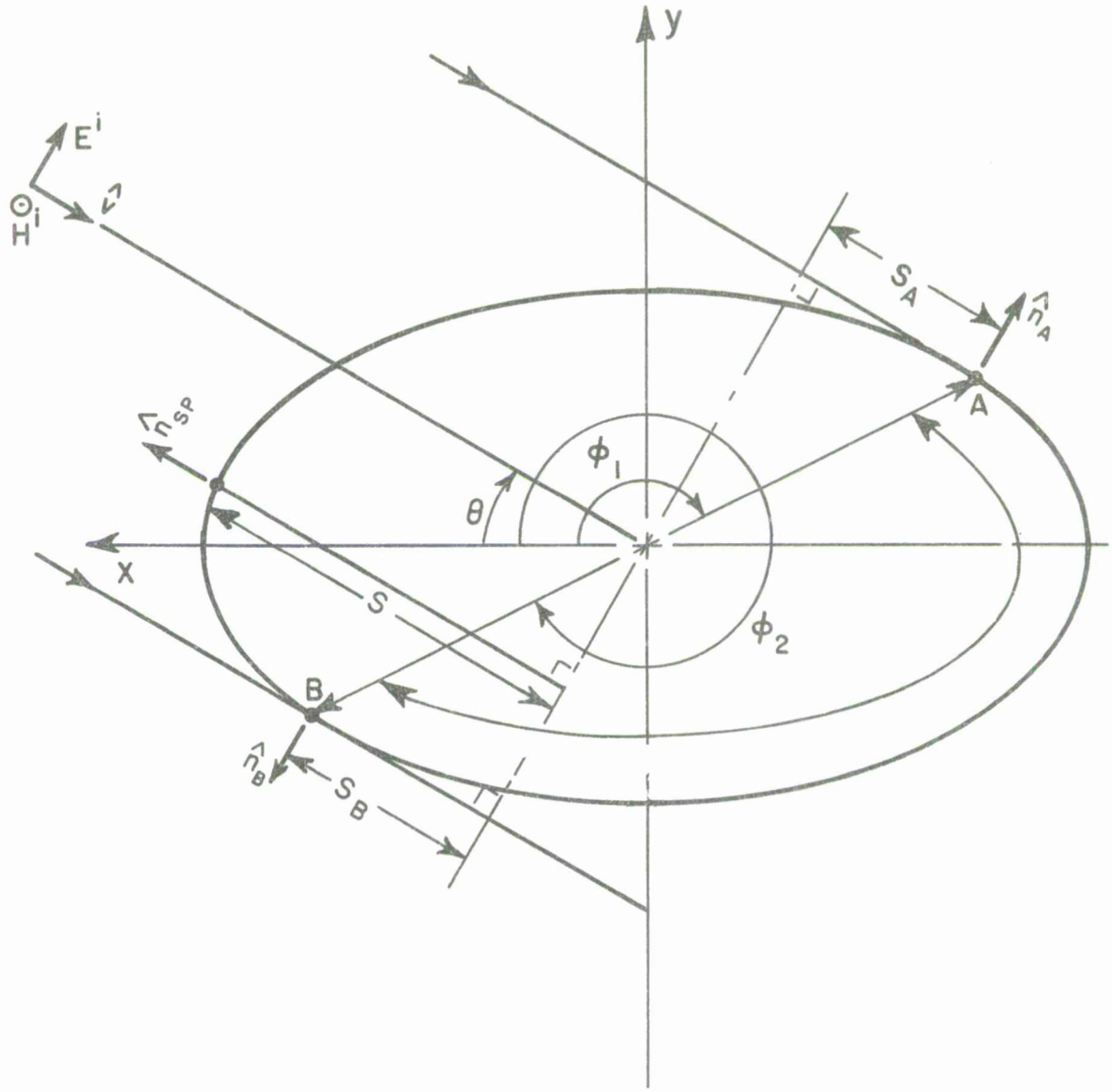

Fig. 10. Scattering of the prolate spheroid.

$$ds = \sqrt{a^2 \sin^2 \phi + b^2 \cos^2 \phi}\, d\phi \quad . \tag{15}$$

Using the form of the diffraction and attenuation coefficients given in Eqs. (4) and (7) and leaving the magnitude of the coefficients open to evaluation using experimental data, one may write the creeping wave as

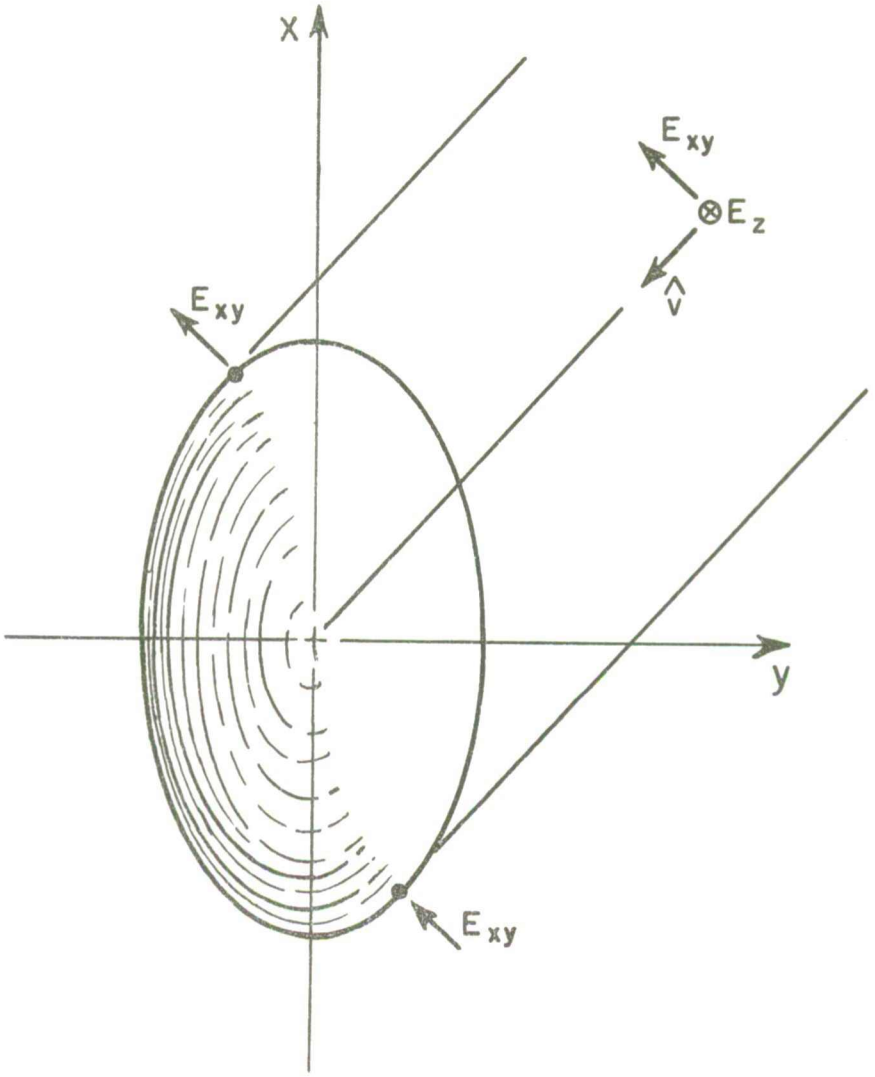

Fig. 11. General incidence angle and polarization scattering by a prolate spheroid.

$$(16) \qquad E_{cw} = 2(U1)\,\rho_A^{\frac{1}{3}}\,\lambda^{\frac{2}{3}}\,e^{-j\frac{\pi}{12}}\,e^{-jk_o\int_{\phi_1}^{\phi_2}\sqrt{a^2\sin^2\phi + b^2\cos^2\phi}\,d\phi}$$

$$\cdot\; e^{-(U2)\,e^{j\frac{\pi}{6}}\lambda^{-\frac{1}{3}}\int_{\phi_1}^{\phi_2}(ab)^{\frac{2}{3}}\frac{d\phi}{\sqrt{a^2\sin^2\phi + b^2\cos^2\phi}}} \cdot \frac{e^{-jk_oR}}{R}\,,$$

where

ρ_A is the local radius of curvature at point A (due to symmetry $\rho_A = \rho_B$)

and the phase reference is taken to be the point (0, 0, 0).

In order to determine the location of the points of attachment and departure A and B for an arbitrary incidence angle we must determine the points on the spheroid where the incident electric field vector is parallel to the normal to the spheroid. This is easily done for the special case illustrated in Fig. 10 through use of the equation of the surface and the cross product of the electric vector and the normal vector; i.e.,

$$(17) \qquad \frac{x^2}{a^2} + \frac{y^2}{b^2} = 1$$

and

$$\hat{n} \times \hat{E}^i = 0\,,$$

where

$$\hat{n} = \frac{\hat{x}\left(\frac{x}{a^2}\right) + \hat{y}\left(\frac{y}{b^2}\right)}{\left[\left(\frac{x}{a^2}\right)^2 + \left(\frac{y}{b^2}\right)^2\right]^{\frac{1}{2}}}$$

and

$$\hat{E}^i = -\hat{x}\sin\theta + \hat{y}\cos\theta\,.$$

Using the above relations two equations in two unknowns are obtained, the unknowns being the x and y coordinates of the attachment points. It is noted that the attachment points are located at $(\mp x_A, \pm y_B)$ because of the symmetry of the body. Solving, one obtains

$$x_{\substack{A \\ B}} = \mp \frac{a^2 \sin\theta}{\sqrt{a^2 \sin^2\theta + b^2 \cos^2\theta}} \tag{18}$$

and

$$y_{\substack{A \\ B}} = \pm \frac{b^2 \cos\theta}{\sqrt{a^2 \sin^2\theta + b^2 \cos^2\theta}} \tag{19}$$

.

Likewise it is necessary to determine the point of specular reflection so that the proper phase between the "physical optics" contribution and the creeping waves can be specified. This is easily done using the relations

$$\frac{x^2}{a^2} + \frac{y^2}{b^2} = 1 \tag{20}$$

and

$$\hat{v} \times \hat{n} = 0,$$

where

$$\hat{v} = \hat{x} \cos\theta - \hat{y} \sin\theta ;$$

which results in

$$x_{sp} = \frac{a^2 \cos\theta}{\sqrt{a^2 \cos\theta + b^2 \sin\theta}} \tag{21}$$

and

$$y_{sp} = \frac{b^2 \sin\theta}{\sqrt{a^2 \cos\theta + b^2 \sin\theta}} \tag{22}$$

.

Thus, referring to Fig. 10, the path length difference between the specular and creeping-wave components can be written as

$$S = + \sqrt{x_{sp}^2 + y_{sp}^2} \quad \cos(\theta - \theta_{sp}) , \tag{23}$$

where

$$\theta_{sp} = \arctan \left| y_{sp} / x_{sp} \right| .$$

Another obstacle to surmount in this analysis is the fact that a closed-form expression of the physical optics contribution for the specular term of the prolate spheroid at arbitrary incidence angles does not exist. Moffatt[12] has derived a time domain solution for the physical optics term by considering the rate of change of cross section that a plane parallel to the incident wavefront encounters as it intercepts the spheroid. This process is illustrated in Fig. 12. Rather than terminating this process at the shadow boundary, as is customary for physical optics, Moffatt terminates the physical optics integral when the maximum cross section is obtained. Transforming, Moffatt's time domain representation and discarding the contribution due to the termination of the integral, as is required in creeping-wave analysis, one may write the "physical optics" (i.e., the specular point) contribution as[17]

$$E_{sp} = - \frac{1}{2} \frac{b^2 a}{b^2 \sin^2\theta + a^2 \cos^2\theta} \left[1 - \frac{1}{j2k\sqrt{b^2 \sin^2\theta + a^2 \cos^2\theta}} \right] \cdot e^{-j2k_o S} . \tag{24}$$

Computation of the total field for the prolate spheroid is now accomplished using Eqs. (6) and (24). However, the computation is not as easy as for that of the sphere because of the presence of the integrals in Eq. (16). In order to perform the integration, numerical integration was employed using a computer program written to calculate the back scattered fields. This computer program is presented in Appendix B. Also, it remains to determine the constants U1 and U2.

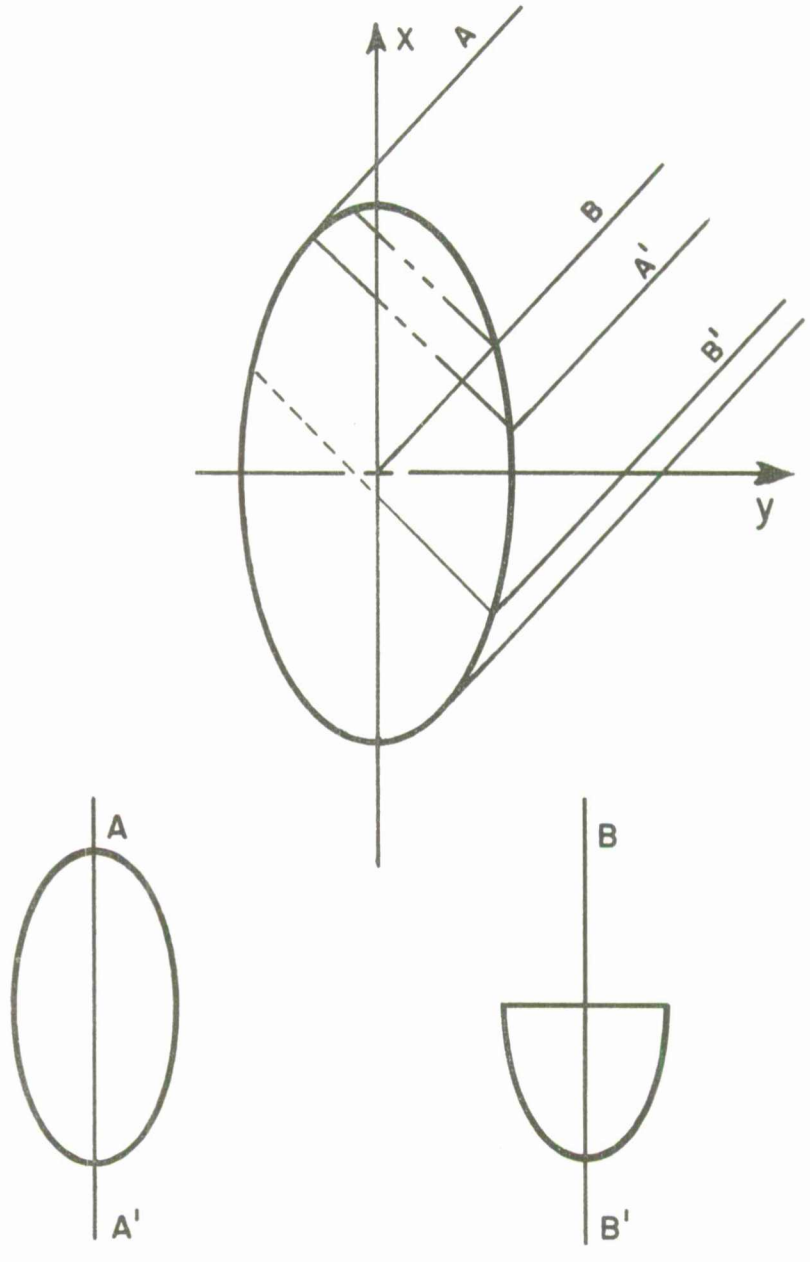

Fig. 12. Physical optics approximation for the prolate spheroid.

The computer program allows an easy determination of the proper values of the parameters U1 and U2 through the process of iteration and comparison.

It seems reasonable to expect that the value U1 for the diffraction constant is comparable to that of the sphere. As a first approximation U1 is taken equal to the value for the sphere, i.e., (0.27). Also it seems reasonable that the value for the attenuation coefficient should be reasonably close to that of the sphere for spheroids of moderate eccentricities. The case of the 2:1 spheroid is examined here since a large amount of data are available for this target. It is of interest to compare the maximum and minimum radii of curvature for a 2:1 prolate spheroid. It is apparent that the maximum and minimum radii of curvature in the x-y plane occur at $\varphi = 0$ and $\pi/2$, respectively. Using Eq. (14) we find that

$$\rho_{min} = \frac{b}{2} \tag{25}$$

and

$$\rho_{max} = 4b ,$$

thus the ratio $\rho_{min} / \rho_{max} = \frac{1}{8}$.

If we define the ratio of the radius of curvature in the direction of propagation of the creeping wave to the orthogonal radius of curvature to be R_α, we have the following correspondence:

Body	R_α	U2
Cylinder	0	1.68
Sphere	1	0.84
2:1 Prolate Spheroid (Parallel Polarization)	$R_{\alpha_{min}} = 1$ $R_{\alpha_{max}} = 4$	Not yet determined

Thus one expects that the value of U2 for the prolate spheroid will be equal to or less than that of the sphere, and may indeed vary along the surface of the spheroid. However, to a first approximation a constant value of U2 will be assumed, since the form of a possible correction term to the attenuation coefficient is not known.

Using the computer program, the back scatter as a function of incidence angle was computed for a range of U2 values for 0.2 to 0.8, and with U1 equal to 0.27. The results of these computations are shown in Fig. 13. It is seen that for $k_o a$ values greater than approximately 3.0, satisfactory results are obtained. However, the present form of the analysis results in a creeping wave contribution which is too large for values of $k_o a$ less than 3.0. As a further check computations over a range of $k_o a$ values were made for the special case (perpendicular polarization) shown in Fig. 14. Here we see that the path traversed by the creeping wave is circular with a value $R_\alpha = 1/2$, and U2 was chosen to be 0.84 as a first approximation. An adaptation of the previous computer program for the sphere was made by using the "physical optics" form for the spheroid. The resultant program is presented in Appendix B. Figure 15 presents the results of this computation, and it is seen that excellent agreement between the computed and measured values is obtained. It is also noted that the curve computed using creeping-wave theory is the same as (within computational accuracy) the curve predicted by Moffatt using time domain analysis.

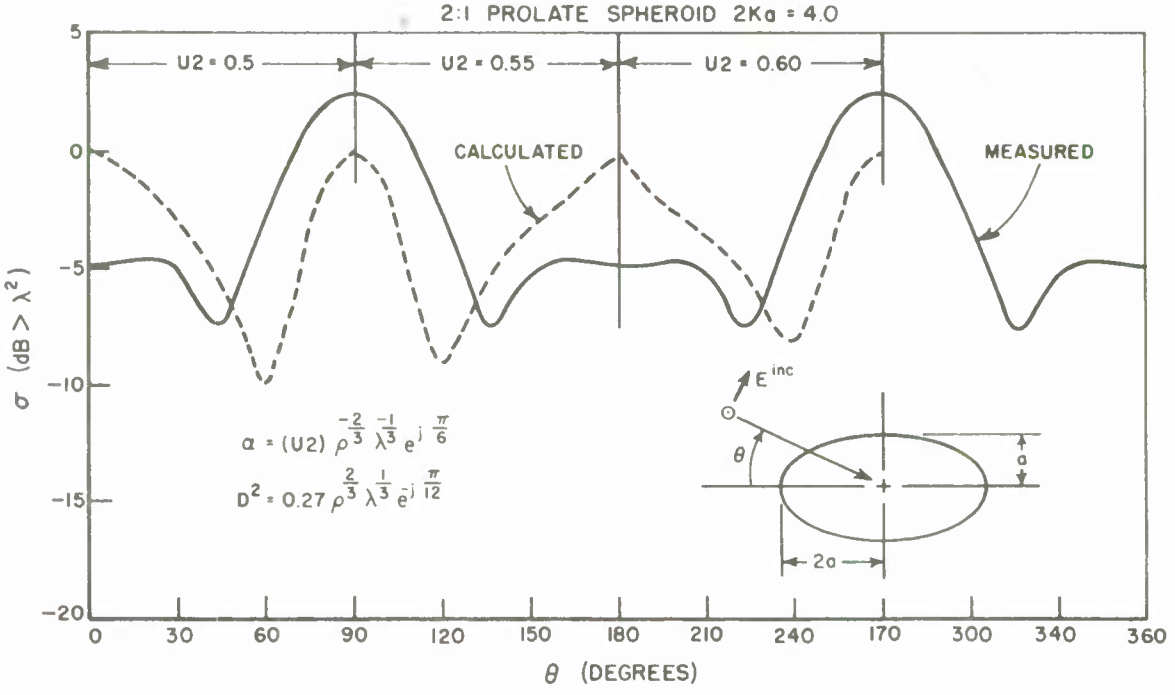

Fig. 13. Backscatter patterns of the prolate spheroid for a range of U2 values (parallel polarization).

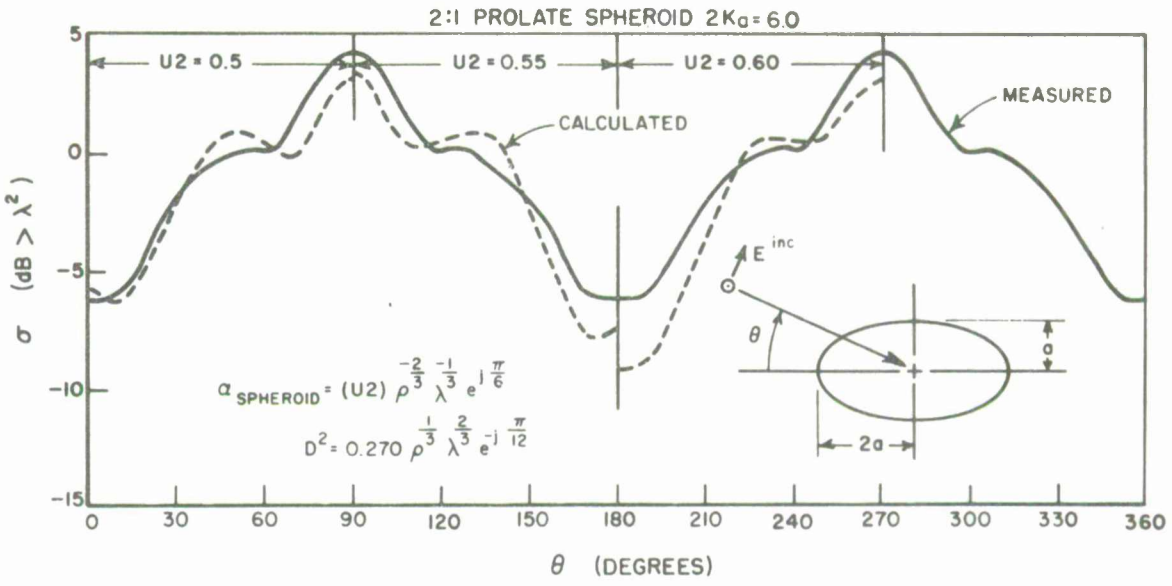

3b

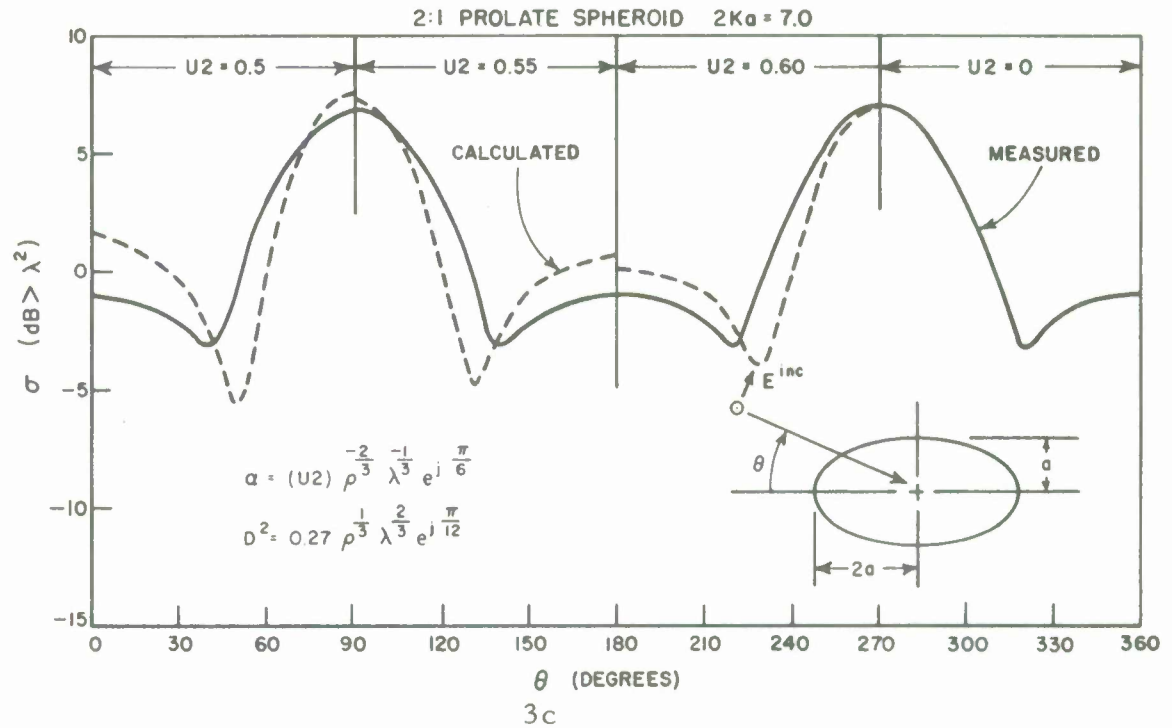

3c

Fig. 13. Backscatter patterns of the prolate spheroid for a range of U2 values (parallel polarization).

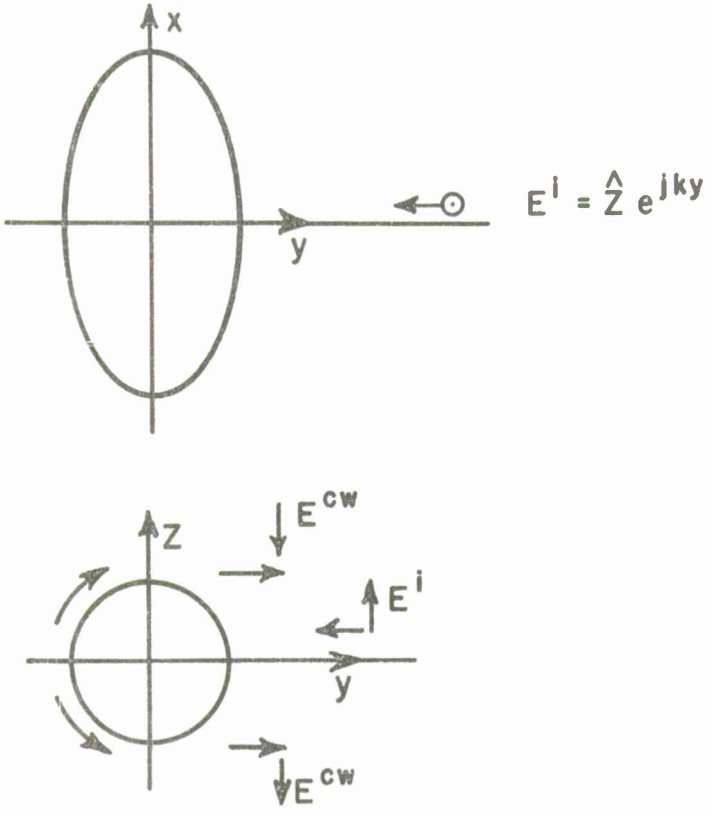

Fig. 14. Scattering by the prolate spheroid for perpendicular polarization and $\theta = 90°$.

From the excellent results of Fig. 15 it would seem that a more accurate calculation of the patterns of Fig. 13 should be possible for small values of $k_o a$. The inaccuracies in Fig. 13 for small values of $k_o a$ are seen to occur in the region about $\theta = 0$ (i.e., nose-on). A possible explanation of these inaccuracies is that the effects of the small radius of curvature at the "nose" of the spheroid are not accurately predicted by a single term in the attenuation coefficient. Another possibility is that a reflection occurs at or near the nose thus decreasing the effect of the creeping-wave fields. Future work should be devoted to extension of the analysis to smaller spheroids and the formulation of a computer program for a general angle of incidence. A goal of this research would be to evaluate the constant associated with the attenuation factor as a function of the ratio of the principal radii of curvature; i.e., a more accurate form for U2 vs. R_α should be found. The values for $R_\alpha = 0$, 1, and ∞ have already been established within reasonable limits.

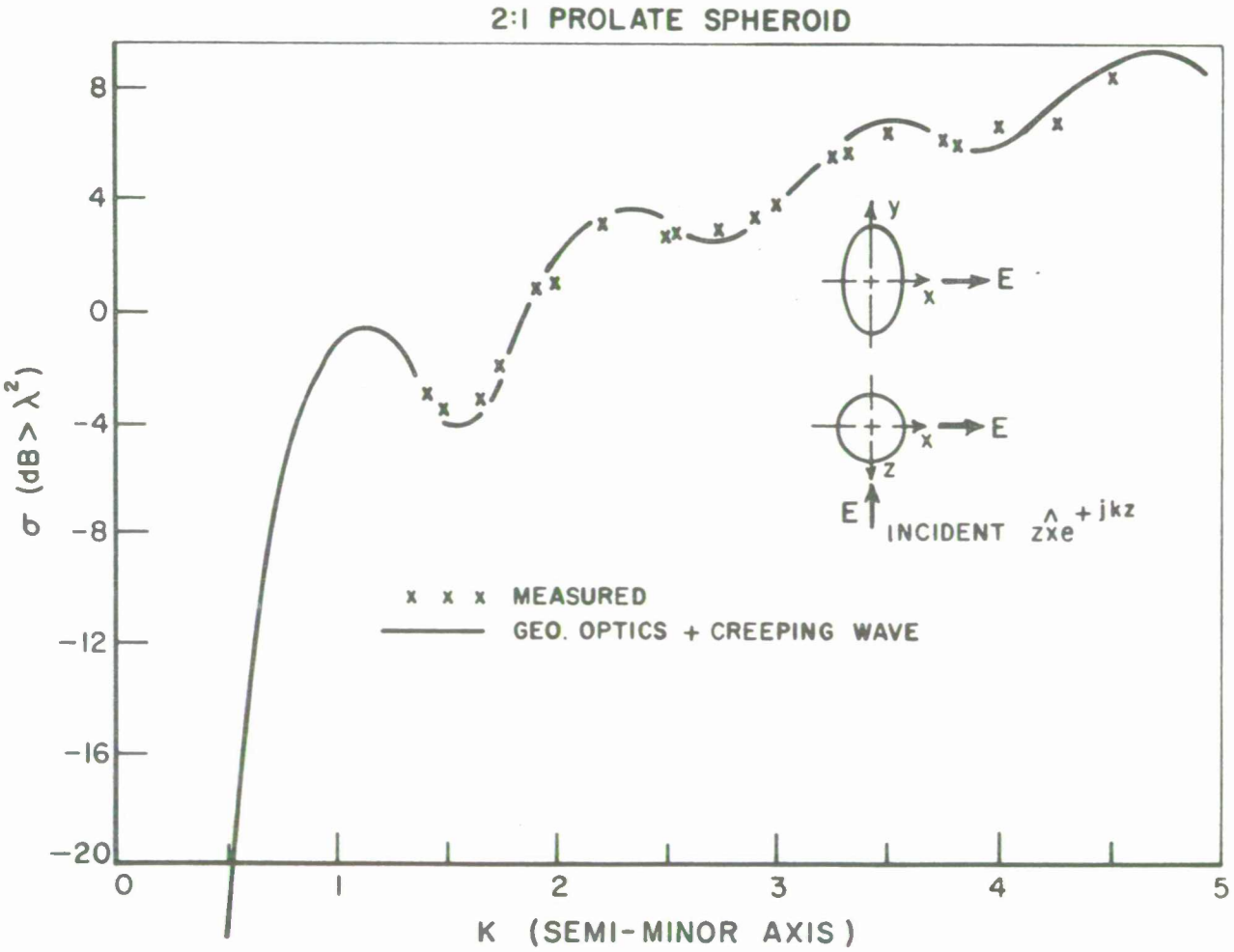

Fig. 15a. Echo area of the prolate spheroid as a function of $k_o a$ for perpendicular polarization and $\theta = 90°$.

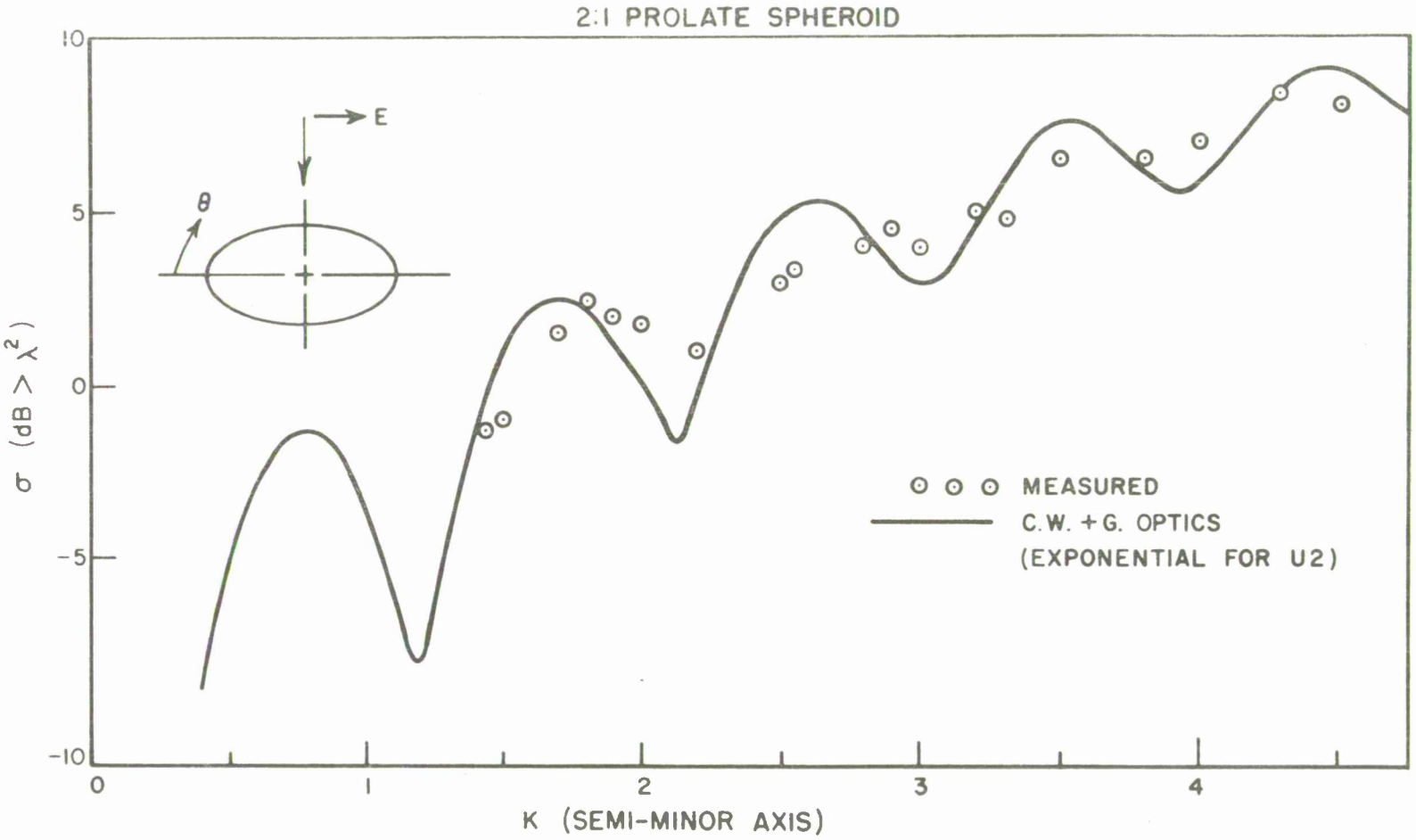

Fig. 15b. Echo area of the prolate spheroid as a function of $k_o a$ for perpendicular polarization and $\theta = 90°$.

C. Analysis of the Ogive and Spherically Capped Ogive in the Near Nose-On Region

The backscatter of the ogive has been treated by Peters[1] using a traveling wave antenna approach. A modification of this traveling wave analysis has been developed by Peters[11] which accounts for radiation losses through use of a creeping-wave attenuation. Cohen[7] experimentally determined values for the reflection at a tip of the ogive. Here we shall show that a consistent picture of scattering by the ogive can be formulated using creeping-wave analysis and application of geometrical theory of diffraction techniques. In particular it is shown that the wedge diffraction coefficient derived by Pauli[18] is applicable to the determination of the tip reflection and transmission coefficients.

Figure 16 shows the ogive and the coordinate system. As in the case of the prolate spheroid, incident energy is trapped at points A and B where the incident electric vector is parallel to the normal to the surface. These creeping waves travel along the ogive until they encounter the tip.

At the tip, part of the creeping-wave energy is diffracted as creeping waves on all geodesics containing the tip and the remainder is radiated from the tip. The previous treatment[11] assumed that the creeping-wave fields on all of the geodesics have equal magnitudes. This is approximately correct but the small differences in the magnitudes will yield the on-axis creeping-wave field which can be observed in the measurements reported by Blore.[19] Off-axis the creeping wave return is a result of the creeping waves which propagate on the ogive in the plane defined by the incidence direction and the incident E-field. In this plane the effect of the tip can be characterized by reflection and transmission coefficients at the tip. Siegel et al[17] have derived an expression for the physical optics scattering by the ogive by assuming that for both monostatic and bistatic returns in the near nose-on region the illuminated tip is the dominant scatterer. Their expression for on-axis backscatter is

$$\sigma(\theta=0) = \frac{\lambda^2 \tan^4\left(\cos^{-1}\frac{h}{r}\right)}{16\pi}, \quad \sqrt{\frac{1}{2kr}} < \cos^{-1}\frac{h}{r} < \frac{\pi}{2} - \sqrt{\frac{1}{2kr}} \qquad (26)$$

Referring to Fig. 16, the backscattered fields attributed to the creeping waves may be written as

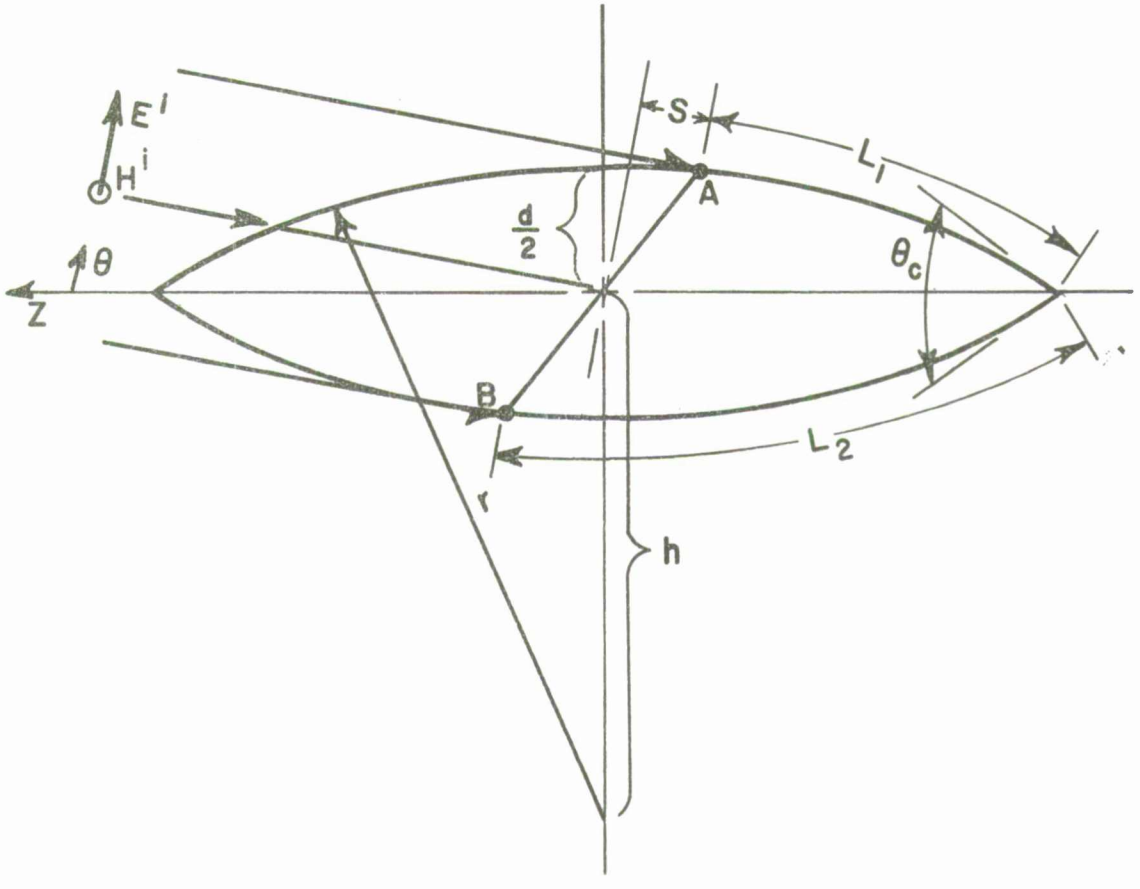

Fig. 16. Coordinate system for the ogive.

$$(27) \qquad E^{cw} = E^{i} \cdot D^{2} \left\{ R_t \left[e^{-(jk_o + \alpha_{og}) \cdot L_1} e^{-j2k_o s} + e^{-(jk_o + \alpha_{og}) \cdot 2L_2} e^{+j2k_o s} \right] + 2\, T_t \left[e^{-(jk_o + \alpha_{og})(L_1 + L_2)} \right] \right\} \frac{e^{-jkR}}{\sqrt{2\pi}\, R} \quad ,$$

where

D is the ogive diffraction coefficient,

R_t is the tip reflection coefficient,

T_t is the tip transmission coeffection,

α_{og} is the ogive attenuation coefficient, and

S, L_1, L_2 are as shown in Fig. 16.

Bistatic radar cross section measurements of the ogive have shown that the energy incident on the tip is scattered by the tip along each geodesic on the ogive; i.e., these tip-scattered fields show no ϕ dependence. This agrees with the results of the equivalent antenna approach, for which no ϕ variation of the field was assumed. Thus a factor of $1/\sqrt{2\pi}$ is introduced to account for the lack of ϕ dependence of the tip-scattered fields. Again attachment points A and B are determined by finding the points on the surface where the normal to the surface is parallel to the incident electric vector. Straightforward analysis results in the relations

$$S = h \sin\theta, \tag{28}$$

$$L_1 = r\left(\frac{\theta_c}{2} - \theta\right), \text{ and}$$

$$L_2 = r\left(\frac{\theta_c}{2} + \theta\right).$$

In the case of the ogive Peters[11] has postulated that the diffraction coefficient remains unchanged from that of the sphere and that the attenuation coefficient is

$$\alpha_{og} = \frac{1}{4}\alpha_s = 0.21\, a^{-\frac{e}{2}} \lambda^{-\frac{1}{3}} e^{j\frac{\pi}{6}} . \tag{29}$$

It is proposed here that the reflection and transmission coefficients be determined using wedge diffraction theory and geometric diffraction theory.

It is seen from Fig. 17a that the tangent planes to the surface at the tip of the ogive, which are normal to the plane defined by the incidence direction and the electric field vector, form a wedge. Using the wedge diffraction formulation of Pauli[18] we write

$$R_t = \sqrt{2\pi kr}\, e^{jkr}\, v_B(r, n, \pi) \tag{30}$$

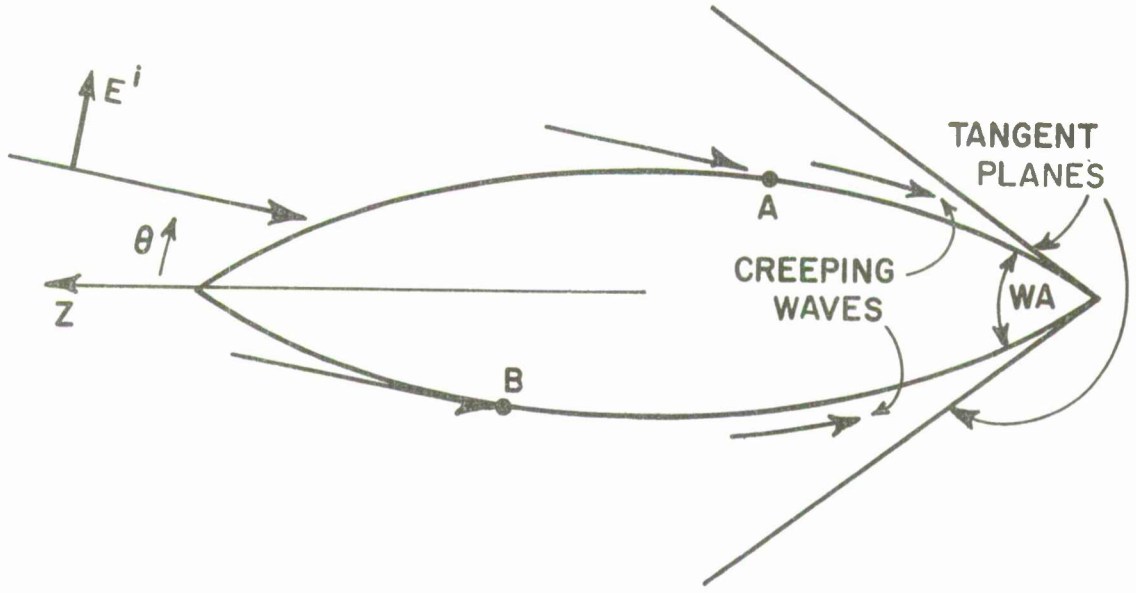

Fig. 17. Tangent planes at the tip of the ogive.

and

$$T_t = \sqrt{2\pi kr}\ e^{jkr}\ v_B(r, n, n\pi) \ ,$$

where

$$n = \frac{1}{\pi}(2\pi - WA)$$

and where the form of v_B given in Eq. (48) for large values of $k_o r$ is employed. Only the relative magnitude of the diffracted fields is utilized, resulting in the multiplication of v_B by the factor $\sqrt{2\pi kr}\ e^{jkr}$. Previously, Cohen[7] had used an experimental approach to determine values of the

reflection coefficient. His method actually determined the sum of the reflected and transmitted components.

The radar cross section for long thin bodies has been derived by considering the body to be an equivalent lossless antenna.[1] The radar cross section of an antenna is

$$\sigma = \gamma^2 \frac{G^2(\theta, \varphi)}{4\pi} \lambda^2 \quad , \tag{31}$$

where

$G(\theta, \varphi)$ is the gain of the antenna,

θ, φ are the far field angles, and

γ is the voltage reflection coefficient at the distant end.

The approximate echo area obtained by this equivalent antenna approach is compared in Fig. 18 to the experimental echo area. The difference between this lossless theoretical picture and experimental values is attributed to a loss mechanism. This loss mechanism could not result

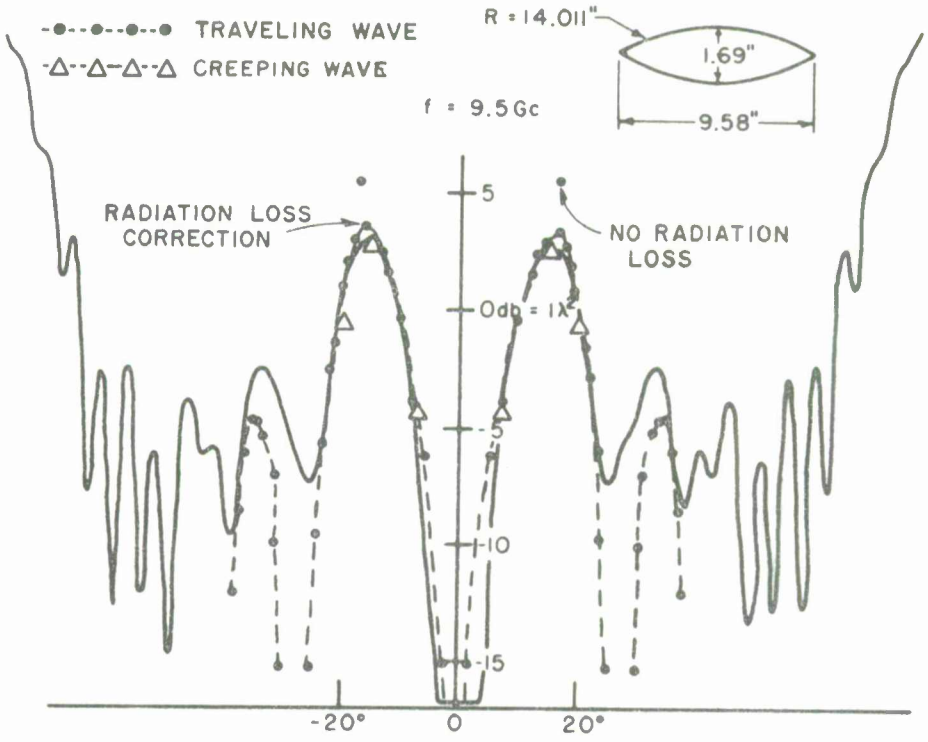

Fig. 18. Backscattered field patterns of the ogive.

from energy absorption since the target is nearly perfectly conducting. It has been shown[11] that this loss mechanism is due to radiation, and that the attenuation coefficient appropriate to determining the loss is that of Eq. (29). Thus the geometrical theory of diffraction solution can be used in the previous equivalent antenna approach to correct the lossless radar cross section computation. Computing the gain pattern, $G(\theta, \phi)$, as in the previous analysis[11,7] and using the ogive attenuation coefficient to correct the gain for radiation loss, one obtains

$$(32) \qquad \frac{\sigma_{loss}}{\sigma_{lossless}} = \left[\frac{e^{-\alpha \ell_1} + e^{-\alpha \ell_2}}{2}\right]^4 .$$

The resultant cross section computed using this correction for radiation loss is shown in Fig. 18 and is seen to be in excellent agreement with the experimental results.

Equation (27) has been used to calculate the maximum scattered fields for ogives having tip angles of 40° and 30° with radii of 11.3λ and 77λ, respectively. A result is shown in Fig. 18. It is seen that satisfactory agreement was obtained in the case of the 40° ogive but the agreement in the case of the 30° angle was not as good. In addition, the scattered fields on-axis were computed using Eq. (33);

$$(33) \qquad E^{cw}_{axis} = E^i D^2 \left\{2R_t\, e^{-(jk_o + \alpha_{og}) \cdot 2L_1} + 2T_t\, e^{(-jk_o + \alpha_{og}) \cdot 2L_1}\right\} \cdot \frac{2\, e^{-jkR}}{\sqrt{2\pi}\, R} .$$

Equation (33) for the on-axis field was obtained by assuming that the form of Eq. (27) holds and that the fields diffracted by the tip in the shadow follow geodesics on the ogive. Also it is assumed that the tip-scattered fields are uniform thus producing a radial field distribution at the shadow boundary. Integration of the contributions around the shadow boundary produces the factor of two difference in Eq. (27) and (33). Results obtained using Eq. (33) were compared with the results obtained by Blore[19] for an ogive with a tip angle of 40° and a radius of 5.65λ. It was found that Eq. (33) did not accurately predict the axial creeping-wave contribution because the magnitude of $|T| - |R|$ was too large. The results of Blore indicate that the on-axis creeping-wave contribution must be of the same order of magnitude as the tip-scattered field, which may be expressed as

$$E^s_{tip} = \frac{\lambda}{8\pi} \tan^2\left(\frac{\theta}{2}\right) . \tag{34}$$

The above results indicate that R_t and T_t are nearly equal, a fact not predicted by wedge diffraction.

Unfortunately R_t and T_t are evaluated for two-dimensional geometry. There is no canonical solution for these diffraction parameters when the wedge is replaced by a cone tip canonical surface. However this approach does explain the presence of the creeping-wave term for the ogive on-axis in that R_t and T_t are different in magnitude, thus resulting in an on-axis creeping-wave contribution, although the resulting contribution is in error. Further theoretical and experimental examination of this problem is required in order to obtain a more accurate solution for the ogive.

Moreland, Peters, and Kilcoyne have applied creeping-wave theory to analysis of a spherically capped ogive as shown in Fig. 19. They have expressed the scattered field as

$$E_s = E^i D^2_{og} e^{-2\gamma_{og} r\theta_o} \left\{ \Gamma \left[e^{-j2k_o\ell + 2\gamma_{og} r\theta} + e^{-2\gamma_{og} r\upsilon} \right] + 2T_{os} T_{so} \left[e^{(jk_o\ell + \gamma_s r_s 2\theta_1 + j\pi)} \right] \right\} \frac{1}{2\pi R} \tag{35}$$

where

$\gamma_{og} = jk_o + \alpha_{og}$,

r = radius of curvature of the ogive,

r_s = radius of the spherical cap,

θ_o, θ_1 = angles shown in Fig. 19,

α_{og} = attenuation coefficient of ogive,

D^2_{og} = diffraction coefficient,

$\gamma_s = jk_o + \alpha_s$, and

α_s = attenuation coefficient of the sphere.

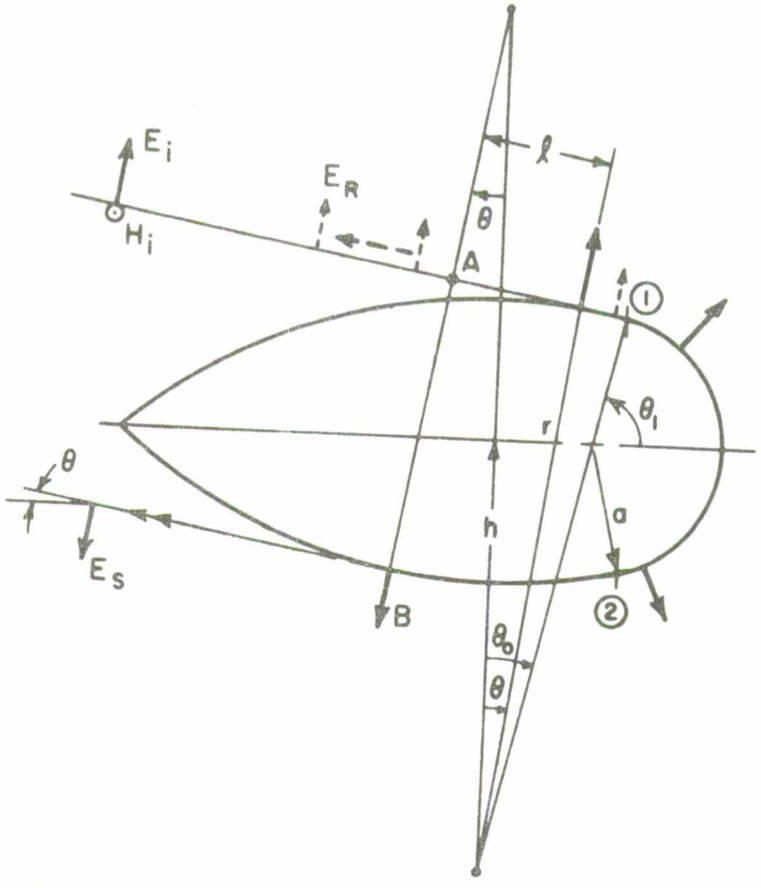

Fig. 19. The spherically capped ogive.

The reflection coefficient, Γ, and the transmission coefficients, T_{os} and T_{so}, arise because of the change of surface impedance at the junction of the ogive and sphere. The surface impedance of the ogive is taken to be Z_o, the impedance of free space, and the surface impedance of the sphere is taken to be the ratio of E_o to H_o for the fields of the major creeping waves postulated in Eqs. (5) and (6) for the sphere. Referring to Fig. 3 we see that this ratio is dependent upon the sphere radius and can be determined from the exact fields of the sphere for a given radius. Thus Γ and T_{os} can be written as

$$\Gamma = \frac{Z_s - Z_o}{Z_s + Z_o} \tag{36}$$

and

$$T_{os} = \frac{2Z_s}{Z_s + Z_o} \tag{37}$$

.

Moreland et al[8] found that it was necessary to assign a negative value to Γ in order to obtain meaningful results, but offered no explanation for this phenomenon. The explanation for the difference in sign between the terms in Eq. (35) is illustrated in Fig. 20 and is explained using geometrical theory of diffraction analysis. It is known that if a ray path encounters a discontinuity in a surface (as shown in Fig. 20) the incident ray is diffracted at the discontinuity giving rise to the existence of a caustic at that point. The case of a "ring" discontinuity, as exists here, introduces a phase shift of $\pi/2$ radians in the ray passing through the discontinuity. Figure 20 , due to Kouyoumjian,[15] illustrates this process. If the process of reflection and transmission of the incident ray is described as follows, it is seen that this phase shift must be taken into account. The process may be described in the following steps: The incident ray, which is bound to the surface, encounters the discontinuity and gives rise to reflected and radiated fields. The reflected field is obtained using Eq. (36). Next the radiated field in the direction of the surface is obtained from the transmission coefficient. The transmitted

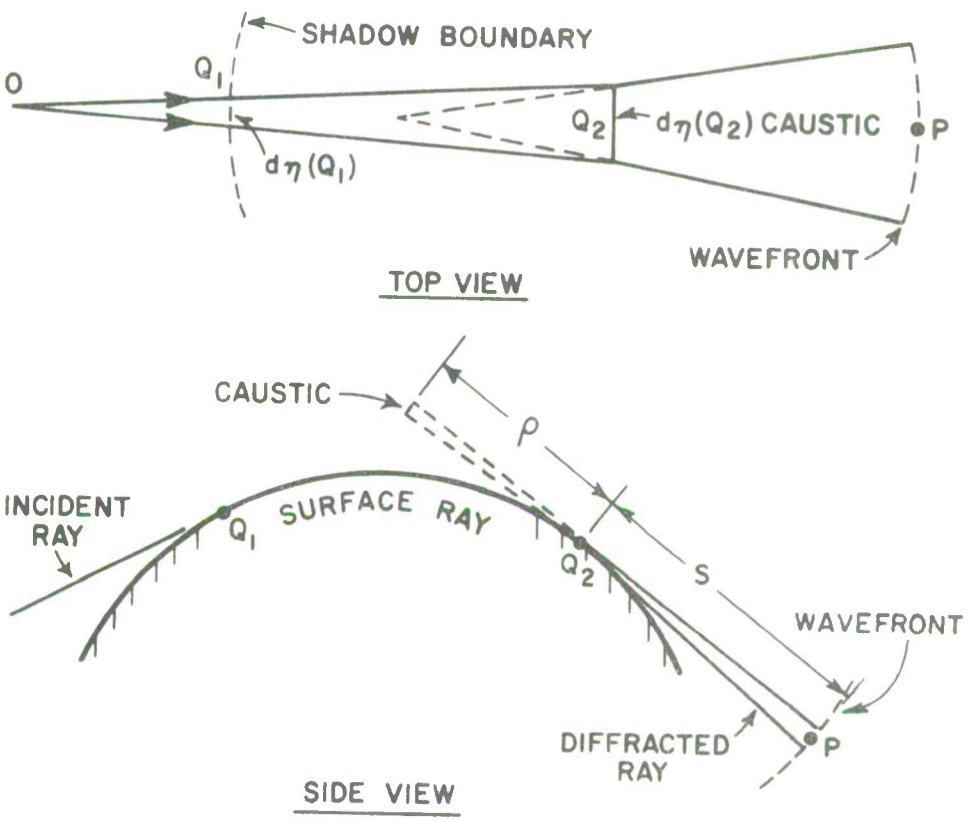

Fig. 20. Diffraction at a surface discontinuity which gives rise to a caustic.

field proceeds through the discontinuity undergoing a phase shift due to the caustic of the radiated rays and re-attaches itself to the surface. Since the transmitted field undergoes this process twice in its travel around the spherically capped ogive, the total phase shift is π radians. In addition, the factor $1/\sqrt{2\pi}$ proposed by Moreland et al is retained to account for the rotational symmetry of the caustic which causes diffracted rays to propagate along the spherical cap in directions other than that of the plane of incidence, thus decreasing the backscattered field. Combining all the terms the total expression for the backscattered field is

$$(38) \qquad E^s = E^i D_{og}^2 e^{-2\gamma_{og} r\theta_o} \left\{ \Gamma \left[e^{-j2k_o\ell + 2\gamma_{og} r\theta} + e^{-2\gamma_{og} r\theta} \right] + 2\, T_{os}\, T_{os} \left[e^{-j(k_o\ell + \gamma_s r_s 2\theta_1 + j2\pi)} \right] \right\} \frac{1}{\sqrt{2\pi R}} \quad .$$

The results of the computation for the spherically capped ogive are presented in Fig. 21 and compared to experimental measurement. It is seen that in the near nose-on region the results are in good agreement with measurement. This form of creeping-wave analysis, coupled with the traveling wave picture and physical optics, allows prediction of the backscattered field of the ogive over a wide range of incidence directions and $k_o a$ values. It should be noted that the impedance of the creeping wave is obtained by a best fit of the fields at the surface of the sphere in the entire shadow region. This would include the fields close to the point at the rear. It has been noted that this is a region of poor fit, regardless of the approximation used, because there are fields present here which are not included in the simple creeping-wave picture. This creeping wave picture, as noted previously, does not include a caustic at the point at the rear. Further improvement in these results would be anticipated if the fields were more closely matched by two creeping waves at a distance removed from the rear point and if multiple interactions are included.

II. CREEPING WAVE ANALYSIS OF PLANAR TARGETS FOR EDGE-ON INCIDENCE

A. The Circular Disk

Ufimtsev[20] and DeVore and Kouyoumjian[21] have treated the circular disk for arbitrary incidence angle and polarization using diffraction techniques. For the case of edge-on incidence with polarization parallel to the

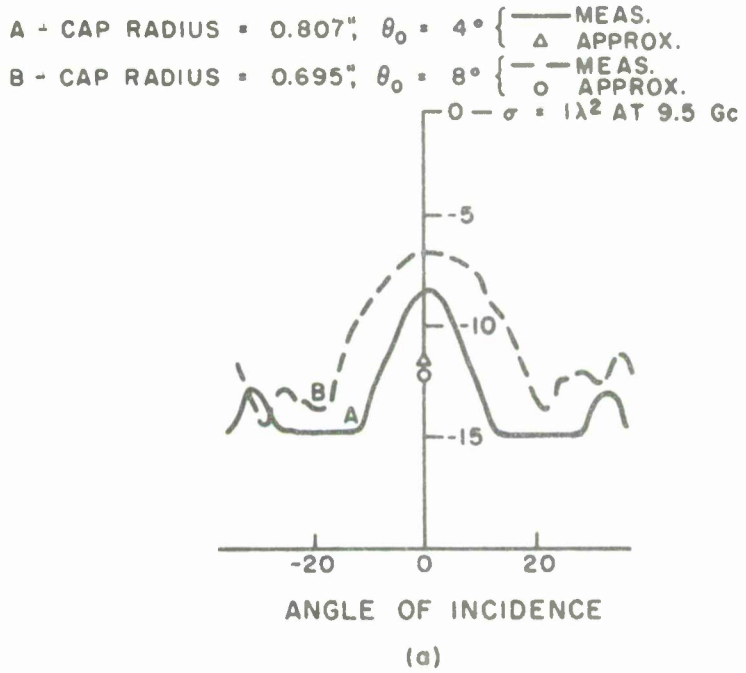

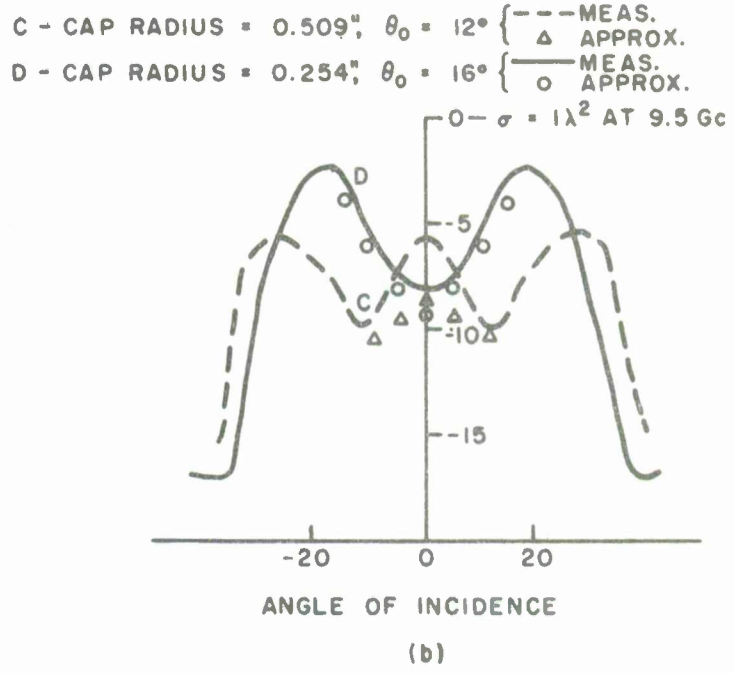

Fig. 21. Backscattered field pattern of the spherically capped ogive.

edge (as shown in Fig. 22) it is possible to construct a solution using creeping-wave concepts. First the specular return is computed by applying geometrical optics in the plane of the disk and edge diffraction in the plane normal to the edge. As seen from Fig. 22, the geometrical optics spreading factor in the plane of the disk can be found by consideration of the reflected rays. It is seen that these reflected rays diverge from the virtual focus located a distance a/2 from the center of the disk. The geometrical optics spreading factor is written as

$$[(\rho_1 \rho_2/(\rho_1 + \ell)(\rho_2 + \ell)]^{\frac{1}{2}}, \quad 15$$

where for plane wave incidence $\rho_1 \to \infty$. In this case ρ_2 is the focal distance a/2 and thus the space attenuation factor becomes $(a/(a+2\ell))^{\frac{1}{2}}$. Combining the space attenuation factor and the result using the edge diffraction coefficient of Appendix A we have, for the backscattered field from the specular point,

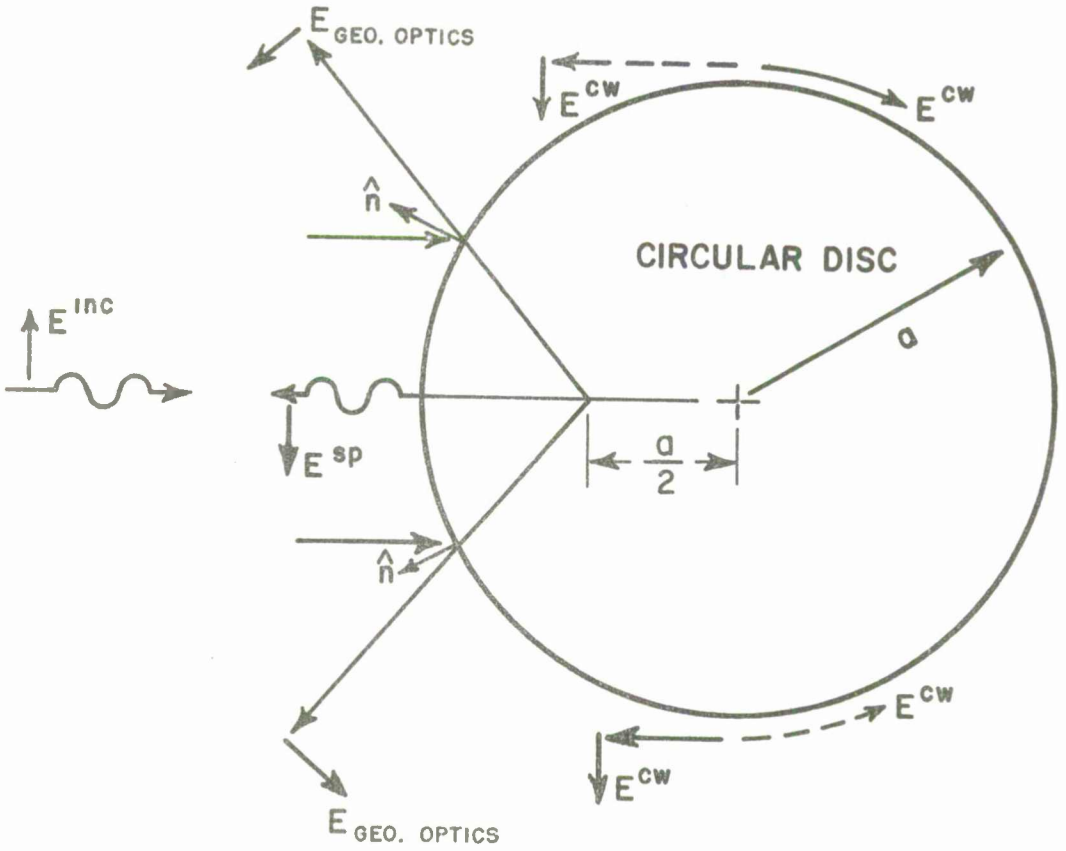

Fig. 22. Scattering by a circular disk edge on.

$$(39) \qquad E_{sp} = -\frac{1}{2}\sqrt{\frac{a}{\pi k}}\; e^{-j\frac{\pi}{4}}\; \frac{e^{-jkR}}{R} \quad .$$

Next it is postulated that two creeping waves travel around the disk, as in the case of the cylinder and sphere. Thus the creeping-wave back-scattered field can be written in the form

$$(40) \qquad E^{cw} = -2D_d^2\, e^{-j2k_o a}\; e^{-(jk_o + \alpha_d)\pi a}\; \frac{e^{-jkR}}{R} \quad .$$

It remains to determine the attenuation and diffraction coefficients which apply to such a target. If the disk is considered to be the limiting case of an oblate spheroid, it is seen that the ratio of the orthogonal radii of curvature at the edge of the disk can be expressed as

$$(41) \qquad R_\alpha = \frac{2a}{b} \quad ,$$

where a and b are shown in Fig. 23.

Now, as the oblate spheroid is "squashed down" into a disk and $b \to 0$ it is seen that the ratio $R \to \infty$. Relating this to the previous ratios of the cylinder, sphere, and ogive it is reasonable to expect that the attenuation coefficient will possess a magnitude U2 on the order of or smaller than that of the ogive. As a first trial a value U2 = 0.21 (i.e., that of the ogive) was chosen. It is more difficult to speculate about the form and magnitude of D_d so the experimental data of DeVore and Kouyoumjiam have been used to determine D_d. The experimental data indicate a deep null in the cross section for a value of $k_o a = 6$. Using Eq. (40) and taking $\alpha_d = \alpha_{og}$ the total field was set equal to zero for $k_o a = 6$. Next it is postulated that D_d^2 is of the same functional form as previously stated. This calculation results in

$$(42) \qquad D_d^2 = 0.0974\; a^{-\frac{1}{3}}\, \lambda^{-\frac{2}{3}}\, e^{-j\frac{\pi}{12}}\, e^{+j\frac{3\pi}{4}} \approx \frac{1}{3} D^2_{sphere}\; e^{+j\frac{3\pi}{4}} \quad .$$

This value of D^2 was then used in connection with the computer program in Appendix B to calculate the curve shown in Fig. 24. In order to check the results for $k_o a$ values larger than those reported by DeVore and Kouyoumjiam, additional measurements were made. These measurements are shown as a range of values because the difficulty in obtaining great

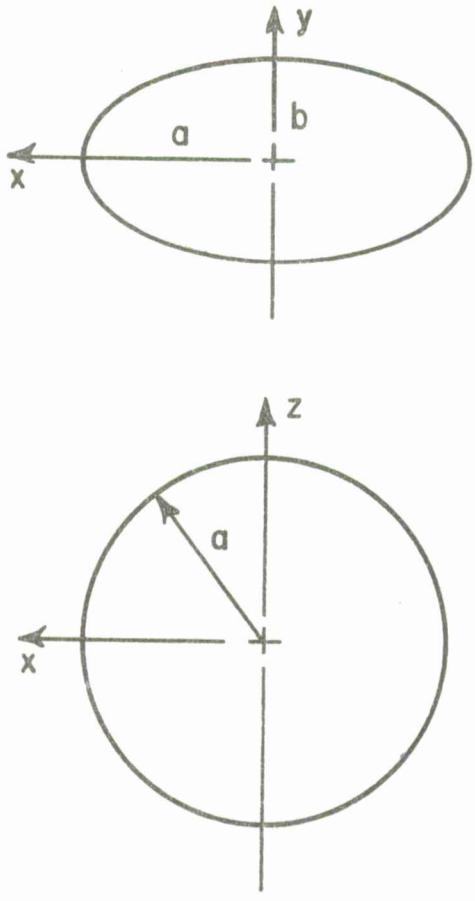

Fig. 23. The oblate spheroid as an approximation to the disk.

precision in the measurements of such low cross section targets. It is seen that this analysis yields results which are in surprising agreement with measurement. It seems reasonable to examine other edge-on configurations to determine if significent creeping-wave contributions are caused by edges.

B. Analysis of the Flat "Ogive"

The analysis of the flat ogive parallels that of the ogive of revolution with the attenuation and diffraction coefficients developed for the disk substituted for the previous ogive attenuation and diffraction coefficients. Again, Pauli's form for wedge diffraction is employed to specify reflection and transmission coefficients at the tip. However, for the case of the flat ogive the tip is treated as a wedge rather than as a point in the determination

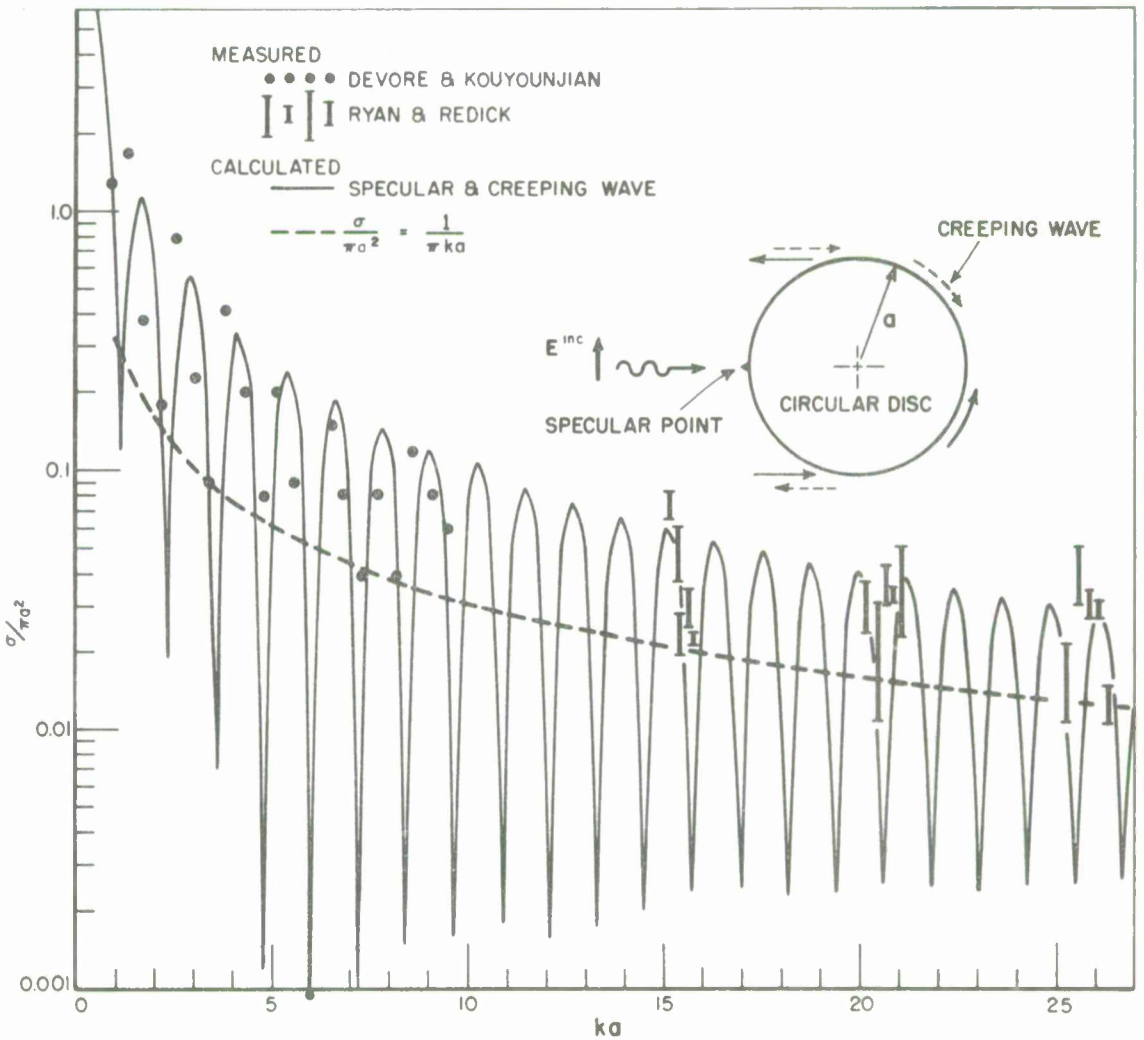

Fig. 24. Backscattering by the circular disk edge one for a range of $k_o a$ values.

of the geometrical optics spreading factor. The wedge diffraction coefficient given in Appendix A accounts for this spreading of rays. The resulting expression for the scattered field is

$$(43) \qquad E^s = E^i D_d^2 \left\{ R_W \left[e^{-(jk_o + \alpha_{og}) \cdot 2L_1} e^{-j2k_o s} + e^{-(jk_o + \alpha_{og}) 2L_2} e^{+j2k_o s} \right] + 2T_W \left[e^{-(jk_o + \alpha_{og})(L_1 + L_2)} \right] \right\} e^{-jkR} ,$$

where

D_d^2 is given by Eq. (42) ,

R_W and T_W are given by Eq. (30) ,

α_{og} is the ogive attenuation coefficient, and

L_1, L_2, and s are shown in Fig. 16 .

Equation (43) has been used to calculate the echo area of the flat ogive and the results are presented in Fig. 25. It is noted that the maximum return of the flat ogive, as measured and calculated, is greater than the return of the ogive of revolution. This is a result of the difference in the geometrical optics spreading at the tip. Whereas the ogive tip diffracts energy into all sectors of three-dimensional space, the flat ogive wedge concentrates the diffracted energy in the plane of the flat ogive. Thus the geometrical optics spreading factors at the tip differ by 2π which compensates for the lower diffraction coefficient of the flat ogive and results in a higher return for the flat ogive. This rather surprising fact is substantiated by the measurements shown in Fig. 25 and it is seen that good agreement between theory and experiment is obtained.

The results of the analysis of the flat ogive indicate that large creeping-wave contributions to the scattered field of a target can result from the presence of edges. This type of creeping-wave contribution is limited to the plane containing the "fin". In scattering directions where the creeping wave on the edge does not contribute, it is possible to obtain an estimate of the scattered field using wedge diffraction techniques.[22,23] At the present time only an estimate is possible because the diffraction coefficient for a finite edge is not known. This estimate is obtained by applying the diffraction coefficient in the plane normal to the edge and

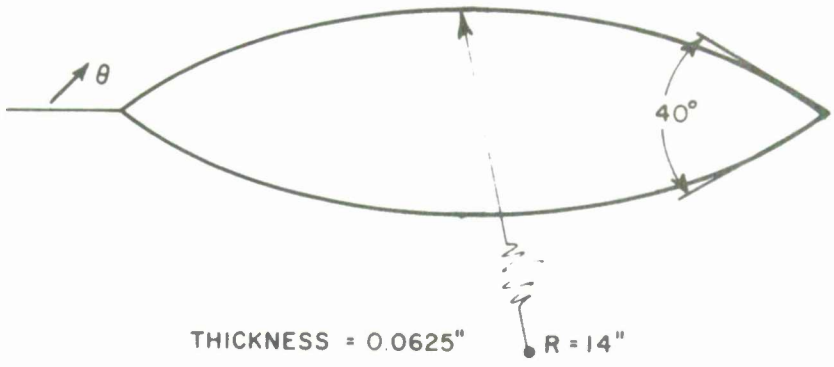

(a)

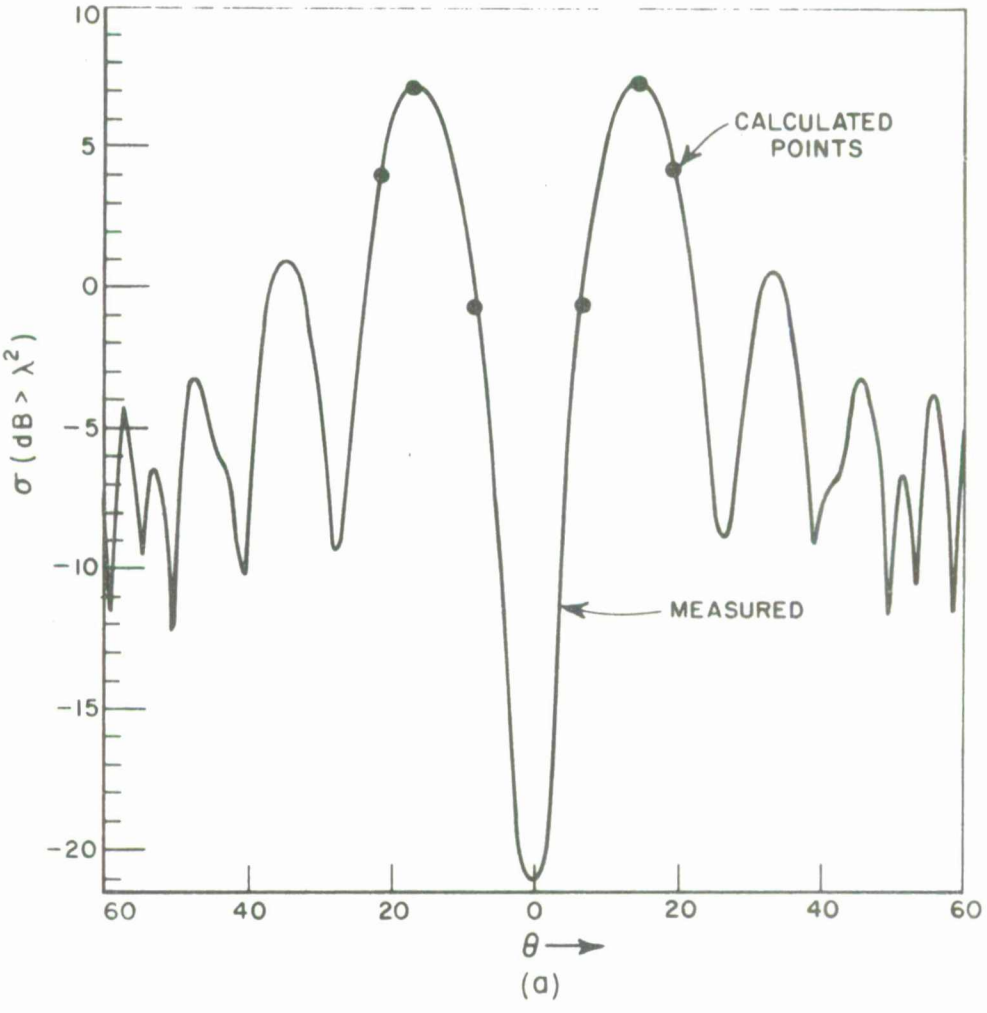

(a)

Fig. 25. Backscatter of the "flat" ogive.

assuming that the edge acts as a traveling wave antenna with constant current excitation in the plane(s) containing the edge.[23] Such an assumption does not meet the boundary condition on a finite edge but does provide an estimate of the maximum scattered field.

Further study of the effects of creeping waves on edges in combination with boundary value techniques may lead to a diffraction type solution for scattering by a finite edge. Such a solution will allow rapid calculation of the effects of the presence of fins and edges on a target.

III. CONCLUSIONS

It has been demonstrated that the geometrical theory of diffraction which incorporates edge diffraction, creeping wave, and geometrical optics techniques can be applied to the problem of scattering by volumetric bodies and edges. In the sample cases considered (spheres, prolate spheroids, ogives, capped ogives, disks, and flat ogives) solutions for the backscattered fields were obtained in simple analytical form. Computation of the backscattered fields using these simple forms is straightforward and takes but a small amount of time on a computer. The nature of the geometrical theory of diffraction solution makes it easy to determine the major scattering centers on a target through the use of ray-tracing techniques and simple computations. Thus a rapid estimate of radar cross section can be obtained for a special case.

Current limitations on this method include the lack of a diffraction solution for scattering by a finite edge, and the unknown dependence of the attenuation and diffraction coefficients on the orthogonal radius of curvature of a solid body. However, results obtained to date indicate that the effects of the orthogonal radius of curvature may be approximated with good accuracy. It also appears that no problem exists for which continued research would not yield a solution. A satisfactory approximation for the scattering by a finite edge seems possible using a combination of diffraction and boundary value techniques. Any problem that cannot be solved analytically can be solved by experimental techniques; e.g., the reflection and transmission coefficients for the ogive. The unifying characteristics of the method offer the expectation that the shadow region geometry of more complex targets could be included in radar cross section solutions, or even that the characteristics of the shadow region could be determined from the measured scattered fields caused by the electromagnetic energy that has propagated through this region.

IV. RECOMMENDATIONS FOR FUTURE RESEARCH

The concept of creeping wave diffraction has been established in this report for geometries that have not been previously considered from this point of view. It remains to obtain more precise values of the diffraction coefficients and attenuation factors for the shapes discussed herein. These efforts should not be restricted to any one approach. Experimental data and modern computational methods such as the point matching boundary value techniques as well as the concepts of wedge diffraction should be used to obtain improved values for these quantities.

Applications of wedge diffraction and the impedance of the creeping wave should be made to evaluate the effects of a discontinuity in the shadow region. Attention should be focused on the exact fields at the surface of the sphere. A serious attempt should be made to reconstruct these fields from the creeping wave point of view. Such studies should yield a more profound understanding of the creeping wave mechanisms and the limitations of this approach. The study should be extended to geometries other than those discussed in this report. An ultimate goal of this approach would be to reduce the computation of the scattered fields of this type to the level that practicing engineers could readily evaluate them or conversely that a generalized computer program could perform this task for a body of general shape.

The applications to antenna theory should not be overlooked. An aircraft is a curved surface. An antenna on such a surface could be effected by such a creeping wave. Ground planes could be terminated in a curved edge. This would reduce irregularities that appear in antenna patterns mounted on such a ground plane. In this case it becomes necessary to separate the diffraction coefficient into its two components as trapping and launching mechanisms do not necessarily occur together, i.e., the antenna parameters would replace one or the other of these on transmission or reception respectively.

ACKNOWLEDGEMENTS

The author wishes to acknowledge the guidance and assistance of Dr. Leon Peters, Jr. and Dr. J.H. Richmond. The work of S.A. Redick in obtaining the measurements is gratefully acknowledged.

APPENDIX A

In order to satisfactorily calculate diffracted rays it is necessary to determine the diffraction of plane and cylindrical waves by a wedge. This has previously been done (see Ref. 24) and an expanded treatment is presented here. Sommerfeld obtained the solution for a perfectly conducting wedge composed of two half-planes with a plane wave incident on the wedge. Sommerfeld also obtained an explicit form of the solution for zero wedge angle; i.e., a half-plane. Pauli[18] determined an explicit form for the general wedge. Oberhettinger[25] presents a different form for the general wedge which he obtained using Green's function techniques.

The diffraction of a cylindrical wave by a wedge is obtained by the use of reciprocity, together with Pauli's expressions for wedge diffraction. Pauli's expressions give the diffraction of a plane wave by a wedge for a general angle of incidence and for polarization either perpendicular or parallel to the edge of the wedge. The total field at observation point P of cylindrical co-ordinates (r, ψ), as shown in Fig. 26, is given by

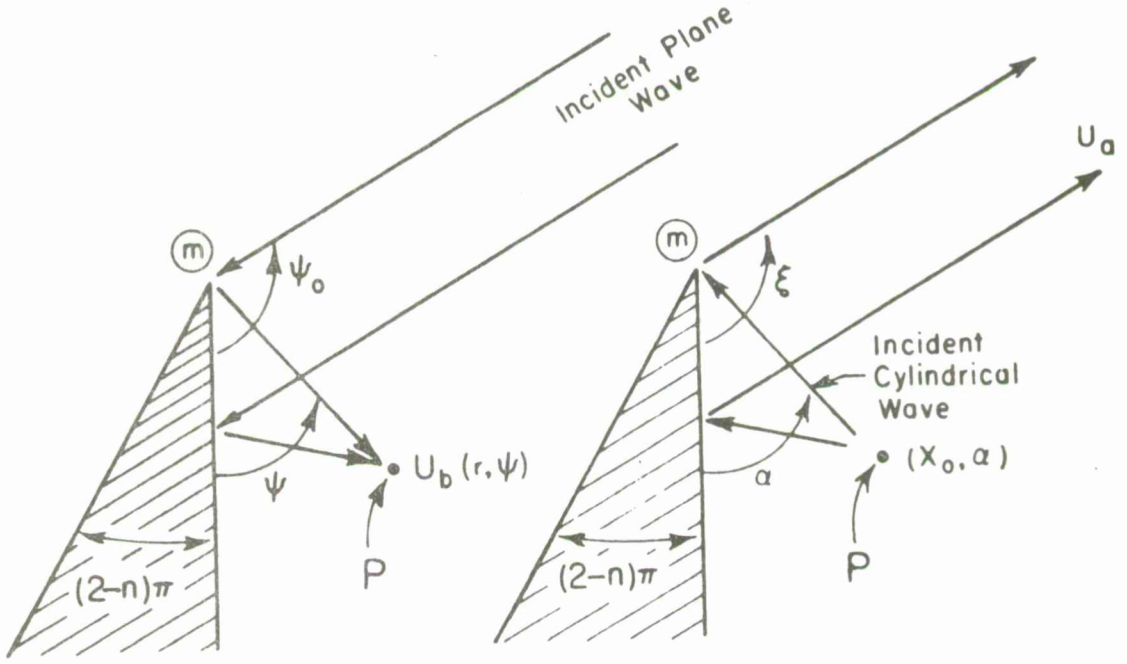

Fig. 26. Diffraction by a wedge of included angle $(2-n)\pi$.

(44) $$u(r, n, \psi) = v(r, n, \psi-\psi_o) \pm v(r, n, \psi+\psi_o)$$

for a plane wave incident from direction ψ_o. The plus sign applies for the polarization of the electric field perpendicular to the edge

$$\left(\frac{\partial u}{\partial n}\bigg|_{edge} = 0\right) \quad ;$$

and the minus sign applies for polarization parallel to the edge $\left(u\big|_{edge} = 0\right)$. The quantities $v(r, \phi)$ are given by

(45) $$v(r, n, \phi) = v^*(r, n, \phi) + v_B(r, n, \phi) \ ,$$

where $v^*(r, n, \phi)$ is the geometrical optics field; and is given by

(46) $$v^*(r, n, \phi) = \begin{cases} \exp[jkr \cos(\phi + 2\pi nN)] \ , & -\pi + 2\pi nN < \phi < \pi + 2\pi nN \\ 0 \qquad \text{otherwise,} \end{cases}$$

where

$$N = 0, \pm 1, \pm 2, \ldots \quad .$$

$v_B(r, n, \phi)$ is the diffracted field for a wedge of angle $WA = (2-n)\pi$; and is given by

(47) $$v_B(r, n, \phi) = \frac{2e^{j\frac{\pi}{4}}}{\sqrt{\pi}} \left(\frac{1}{n} \sin \frac{\pi}{n}\right) \frac{\left|\cos \frac{\phi}{2}\right|}{\cos \frac{\pi}{n} - \cos \frac{\phi}{n}}$$

$$\cdot \ e^{jkr \cos \phi} \int_{\sqrt{akr}}^{\infty} e^{-j\tau^2} \, d\tau$$

$$+ \ldots \ ,$$

where $a = 1 + \cos \phi$.

Equation (47) is composed of a leading term plus higher-order terms which are negligible for large values of kr. For large values of (akr) Eq. (47) becomes

$$(48) \qquad v_B(r, n, \phi) = \frac{e^{-j(kr + \pi/4)}}{\sqrt{2\pi kr}} \quad \frac{\frac{1}{n} \sin \frac{\pi}{n}}{\cos \frac{\pi}{n} - \cos \frac{\phi}{n}} + \ldots \quad .$$

The diffracted field, as expressed by Eq. (48), is that from which the asymptotic diffraction coefficients of the geometrical theory of diffraction are obtained.[26] Since this expression is valid only for large values of (akr), it is not valid on the shadow boundary because a = 0 there. Then Eq. (47) must be used, which gives the value of the diffracted field on the shadow boundary as

$$(49) \qquad v_B(r, n, \pi) = \mp \frac{1}{2} e^{-jkr} + \ldots$$

$$\begin{cases} \text{upper sign for } \phi = \pi^- \\ \text{lower sign for } \phi = \pi^+ \end{cases} \quad .$$

The value of $v(r, \phi)$ on the shadow boundary can then be obtained from Eqs. (45), (46), and (49) as

$$(50) \qquad v(r, n, \pi) = \frac{1}{2} e^{-jkr} + \ldots \quad ,$$

which is one-half of the incident field on the illuminated side of the shadow boundary.

The series representation of v_B given in Eq. (45) is valid everywhere except for the values

$$(51) \qquad \phi = \pm \pi + 2\pi nN, \quad n \neq 2, \quad N = \pm 1, \pm 2, \ldots \quad .$$

Near these values the series representation converges slowly, and the periodicity property of the exact function $v(r, n, \phi)$ can be used to overcome convergence difficulties near these values. The exact function $v(r, n, \phi)$ is periodic in $2\pi n$ so that

(52) $$v(r, n, \phi + 2\pi nN) = v(r, n, \phi), \quad N = 0, \pm 1, \pm 2, \ldots .$$

Therefore, if the series representation of v_B converges slowly because ϕ is near one of the values expressed by $N \neq 0$ in Eq. (51), the periodicity property of Eq. (52) can be used to represent $v(r, \phi)$ by employing the series representation near $\phi = \pm \pi (N = 0)$. The only case for which all boundaries are regular and the substitution of Eq. (52) is not necessary is for the thin half-plane, in which case $n = 2$.

We now examine the behavior of the diffraction coefficient $v_B(r, n, \phi)$ for the case illustrated in Fig. 27 in which two reflected rays exist at angles ψ_1 and ψ_2. We first examine the values of $\phi = \psi + \psi_o$ for the diffracted rays corresponding to the directions of these reflected rays.

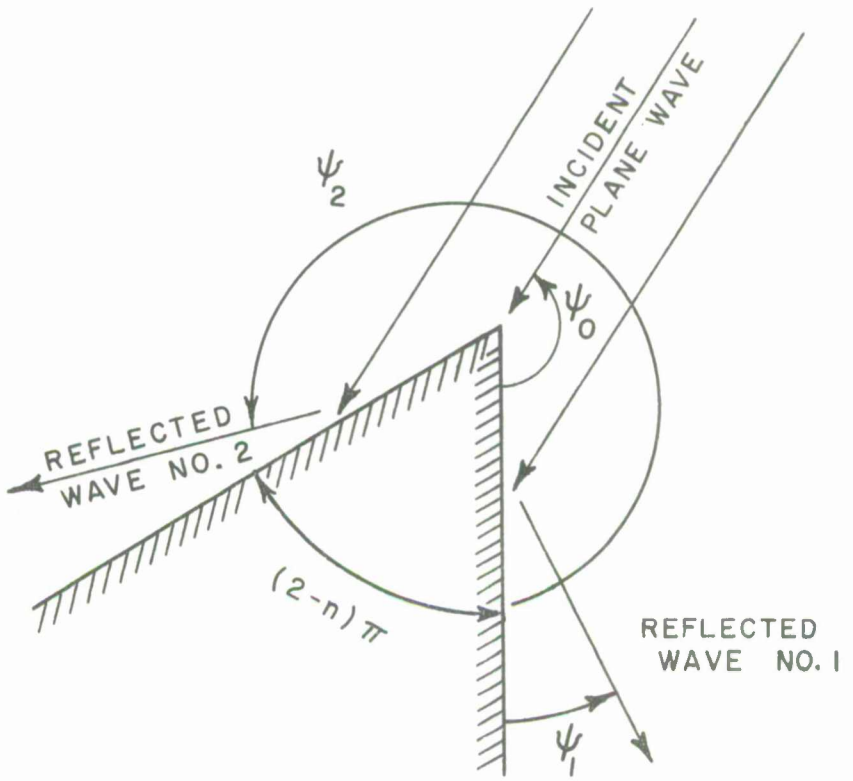

Fig. 27. Case of diffraction by a wedge where two reflected rays exist.

The values of the pertinent angles are

$$(53) \qquad \psi_1 = \pi - \psi_o , \qquad \psi_2 = (2n\pi - \pi) - \psi_o .$$

Thus the values of $\phi = \psi + \psi_o$ are

$$(54) \qquad \phi_1 = \pi , \qquad \phi_2 = (2n\pi - \pi) .$$

For $\phi_1 = \pi$ Eq. (47) expresses the value of the diffraction coefficient and thus the total field at $\psi = \psi_1$ is one-half the geometrical optics reflected field on the illuminated side of the shadow boundary, as given by Eq. (50).

However, for $\phi_2 = 2n\pi - \pi$ and $n \neq 2$, Eq. (47) is not analytic and consequently the following substitution is made:

$$(55) \qquad v(r, n, \phi) \rightarrow v(r, n, \phi - 2\pi n)$$

for values of

$$(56) \qquad \phi > \pi n .$$

The region over which the subtitution of Eq. (55) is made, as expressed by Eq. (56), is determined from the symmetry property of $v(r, n, \phi)$; i.e.,

$$(57) \qquad v(r, n, -\phi) = v(r, n, +\phi) .$$

That is, if the substitution of Eq. (55) is made for values of $\phi < \pi n$, then the substituted values of $\phi - 2\pi n$ are closer to the value of non-analyticity $\pi - 2n\pi$ than the original values of ϕ were to the value of non-analyticity $2n\pi - \pi$. It is also noted that the value substituted for $v(r, n, \phi_2)$ is $v(r, n, -\pi)$, which corresponds to the correct value for a shadow boundary.

The equations given in this Appendix apply for plane-wave incidence, but they can be used for cylindrical-wave incidence as shown below. Consider the two situations shown in Fig. 26. It is desired to find the field u_a

in some direction ξ for the wedge illuminated by a cylindrical wave with its source located at (x_o, α). By reciprocity the field u_a is equal to the field u_b which is located at the point $(r = x_o, \psi = \alpha)$ and with a plane wave incident from the direction $\psi_o = \xi$. The value of u_b is given by Eq. (47). Thus using the property expressed in Eq. (44) the solution for diffraction of a cylindrical wave by a wedge becomes

$$u_a = v(x_o, n, \xi + \alpha) \pm v(x_o, n, \xi - \alpha) \quad . \tag{58}$$

The field at infinity is given by Eq. (58) for a perfectly conducting wedge illuminated by the line source at (x_o, α).

If the quantity (akx_o) is sufficiently large for Eq. (48) to be valid, then the diffraction pattern for cylindrical-wave incidence has the same form as that for plane-wave incidence. In other words, the diffraction for cylindrical-wave incidence is the same as that for plane-wave incidence in regions sufficiently removed from the shadow boundaries. The region near the shadow boundary in which Eq. (47) must be used increases for decreasing values of x_o and may encompass all 360 degrees.

APPENDIX B
A LISTING OF COMPUTER PROGRAMS USED IN THE PREPARATION OF THIS REPORT

These programs are coded in SCATRAN, an automatic compiler language developed by the Numerical Computation Center of The Ohio State University. SCATRAN is similar to FORTRAN IV in the form of arithmetic expressions used. An experienced programmer can easily translate these SCATRAN programs into any desired language.

```
 ***          RUN
 ***          DUMP LOWER CORE
 ***          SCATRAN
C             DIFFRACTION ANALYSIS OF BACKSCATTER BY A CIRCULAR DISC-EDGE
              ON-
C             OGIVE ATTENUATION AND DIFFRACTION COEFFICIENTS USED-
C             WAVELENGTH=1.-
              COMPLEX(E1,E2,E3,E4,E5,CEXPL,,DSQ,ALPH,X5,ECW,ECWT,ETOT)-
              COMPLEX(E6)-
  START       P1=3.1415927-
              TP=2.*P1-
              U1=0.0974-
              U2=0.210-
              R13=1./3.-
              R23=2./3.-
              P16=P1/6.-
              P112=P1/12.-
              READINPUT,8,(NKA)-
              WRITEOUTPUT,3,(NKA)-
              READINPUT,7,(SFKA,DELKA)-
              WRITEOUTPUT,2,(SFKA,DELKA)-
              WRITEOUTPUT,2-
              E1=COS.(P112)-.1.SIN.(P112)-
              E2=COS.(P16)+.1.SIN.(P16)-
              E6=COS.(P14)-.1.SIN.(P14)-
              DOTHROUGH(S100),I=1.1.1.LE.NKA-
              FI=I-1-
              FKA=SFKA+FI*DELKA-
              A=FKA/TP-
              F1=FLPFL.(A,R13)-
              DSQ=U1*F1*E1-
              F2=1./FLPFL.(A,R23)-
              ALPH=U2*F2*E2-
              X3=2.*FKA-
              E3=COS.(X3)-.1.SIN.(X3)-
              FL=P1*A-
              FLK=P1*FKA-
              E4=COS.(FLK)-.1.SIN.(FLK)-
              X5=-FL*ALPH +.1.0.-
              E5=CEXPL.(X5)-
              ECW=DSQ*E3*E4*E5-
              ECWT=2.*ECW-
              ESP=-(SQRT.(A/2.))/TP-
              ESP=ESP*E6-
              ETOT=ESP-ECWT-
              Y1=.REAL.ETOT-
              Y2=.IMAG.ETOT-
              FETSQ=(Y1*Y1)+(Y2*Y2)-
              SIGMA=4.*FETSQ/(A*A)-
              WRITEOUTPUT,2,(FKA,DSQ,ALPH,ETOT,SIGMA)-
              WRITEOUTPUT,2-
  S100        CONTINUE-
              CALLSUBROUTINE()=ENDJOB.()-
              ENDPROGRAM(START)-
 ***          DATA
00500
0.1         0.1
```

```
M**          RUN
***          DUMP LOWER CORE
***          SCATRAN
C            DIFFRACTION ANALYSIS OF BACKSCATTER BY A SPHERE -
C            A CHECK ON REPORT OSURF 1815-5-
C            WAVELENGTH=1.-
             COMPLEX(E1,E2,E3,E4,E5,CEXPL..DSQ,ALPH,X5,ECW,ECWT,ETOT,EPO
              )-
  START      PI=3.1415927-
             TP=2.*PI-
             U1=0.270-
             U2=0.210-
             R13=1./3.-
             R23=2./3.-
             P16=PI/6.-
             P112=PI/12.-
             RADEG=57.29578-
             READINPUT.8.(NKA)-
             WRITEOUTPUT.3.(NKA)-
             READINPUT.7.(SFKA.DELKA)-
             WRITEOUTPUT.2.(SFKA.DELKA)-
             WRITEOUTPUT.2-
             E1=COS.(P112)-.1.SIN.(P112)-
             E2=COS.(P16)+.1.SIN.(P16)-
             DOTHROUGH(S100).I=1.1.I.LE.NKA-
             FI=I-1-
             FKA=SFKA+FI*DELKA-
             A=FKA/TP-
             F1=FLPFL.(A.R13)-
             DSQ=U1*F1*E1-
             F2=FLPFL.(FKA.R13)-
             X1=0.750*PI-
             F3=FLPFL.(X1.R23)-
             ALPH=F2*F3*E2/(4.*A)-
             X3=2.*FKA-
             E3=COS.(X3)-.1.SIN.(X3)-
             FL=PI*A-
             FLK=PI*FKA-
             E4=COS.(FLK)-.1.SIN.(FLK)-
             X5=-FL*ALPH +.1.0.-
             E5=CEXPL.(X5)-
             ECW=DSQ*E3*E4*E5-
             ECWT=2.*ECW-
             EPO=-0.5*A-.1.A/(4.*FKA)-
             ETOT=EPO-ECWT-
             Y1=.REAL.ETOT-
             Y2=.IMAG.ETOT-
             FETSQ=(Y1*Y1)+(Y2*Y2)-
             SIGMA=4.*FETSQ/(A*A)-
             Y3=.REAL.ECWT-
             Y4=.IMAG.ECWT-
             FMECW=SQRT.(Y3*Y3+Y4*Y4)-
             PHECW=FATAN2.(Y4.Y3)-
             PHDEC=RADEG*PHECW-
             WRITEOUTPUT.2.(FKA.SIGMA.EPO.ETOT.FMECW.PHDEC)-
             WRITEOUTPUT.2-
  S100       CONTINUE-
             CALLSUBROUTINE()=ENDJOB.()-
             ENDPROGRAM(START)-
 ***         DATA
00500
0.1        0.1
```

```
 ***          RUN
 ***          DUMP LOWER CORE
 ***          SCATRAN
C             DIFFRACTION ANALYS)S OF BACKSCATTER BY A SPHERE -
C             A CHECK ON REPORT OSURF )8)5-5-
C              BISTATIC SCATTER OF A SPHERE-
C             WAVELENGTH=1.-
              COMPLEX(E1,E2,CEXPL,,DSQ,ALPH,ECW,ECWT,ETOT,EPO)-
              COMPLEX(ALPH),ALD1,ALD2,EXL,EXL),EXL2)-
   START      PI=3.)415927-
              TP=2.*PI-
              U1=0.270-
              U2=0.210-
              R13=1./3.-
              R23=2./3.-
              PI6=PI/6.-
              PI)2=PI/)2.-
              RADEG=57.29578-
              READ INPUT,8,(NKA,NTHETA)-
              WRITE OUTPUT,3,(NKA,NTHETA)-
              READ INPUT,7,(SFKA,DELKA,THETS,DELTH)-
              WRITE OUTPUT,2,(SFKA,DELKA,THETS,DELTH)-
              WRITEOUTPUT,2-
              E)=COS.(PI12)-.1.SIN.(PI12)-
              E2=COS.(PI6)+.1.SIN.(PI6)-
              DO THROUGH(S100),J=),1,J.LE.NTHETA -
              FJ=J-)-
              THETD=THTS+FJ*DELTH-
              THETA=DEGRAD*THETD-
              THET2=PI-THETA-
              THET3=THET2/2.-
              WRITE OUTPUT,FMT),(THETD)-
F  FMT)       (5X,9*BISTATIC ANGLE = *,F)5.8)-
              WRITE OUTPUT,FMT2-
F  FMT2       ()20H      KA              S)GMA          REEPO          IMEPO
                         RETOT           IMETOT         FMECW          PHDEC
                   )-
              DOTHROUGH(S100),)=),),1.LE.NKA-
              FI=)-)-
              FKA=SFKA+FI*DELKA-
              A=FKA/TP-
              FK=FKA/A-
              FI=FLPFL.(A,R13)-
              DS0=U)*F)*E)-
              F2=FLPFL.(FKA,R13)-
              X)=0.750*PI-
              F3=FLPFL.(XI,R23)-
              ALPH=F2*F3*E2/(4.*A)-
              COS3=COS.(THET3)-
              EPO=(-),-.1.COS.(THET2)/(2.*FKA*COS3*COS3*COS3))*0.5*A-
              DL=A*SIN.(THET2)-
              D2KL=2.*FK*DL-
              ALPH)=ALPH+.1.FK-
              DL)=A*THETA-
              DL2=(TP-THETA)*A-
              ALD)=-ALPHI*DL)-
              ALD2=-ALPHI*DL2-
              EXL=COS.(D2KL)-.1.SIN.(D2KL)-
              EXL)=CEXPL.(ALD))-
              EXL2=CEXPL.(ALD2)-
              ECWT=-DSQ*EXL*(EXLI+EXL2)-
              ETOT=EPO+ECWT-
              YI=.REAL.ETOT-
              Y2=.IMAG.ETOT-
```

```
                FETSQ=(Y1*Y1)+(Y2*Y2)-
                SIGMA=4.*FETSQ/(A*A)-
                Y3=.REAL.ECWT-
                Y4=.IMAG.ECWT-
                FMECW=SORT.(Y3*Y3+Y4*Y4)-
                PHECW=FATAN2.(Y4,Y3)-
                PHDEC=RADEG*PHECW-
                WRITEOUTPUT.2.(FKA,SIGMA,EPO,ETOT,FMECW,PHDEC)-
                WRITEOUTPUT.2-
      S100      CONTINUE-
                CALLSUBROUTINE()=ENDJOB.()-
                ENDPROGRAM(START)-
      ***       DATA



      ***       RUN
      ***       DUMP LOWER CORE
      ***       SCATRAN
C               BACKSCATTER FROM A PROLATE SPHEROID-
C               SCATTERING IN THE PLANE 90 DEGREES FROM THE MAJOR AXIS-
C               WAVELENGTH=1.-
                COMPLEX(E1,E2,E3,E4,E5,CEXPL..DSQ,ALPH,X5,ECW,ECWT,ETOT,EPO
                  )-
      START     PI=3.1415927-
                TP=2.*PI-
                U1=0.270-
                U2=0.210-
                R13=1./3.-
                R23=2./3.-
                P16=PI/6.-
                P112=PI/12.-
                RADEG=57.29578-
                RATIO=2.-
                READINPUT.8.(NKA)-
                WRITEOUTPUT.3.(NKA)-
                READINPUT.7.(SFKA,DELKA)-
                WRITEOUTPUT.2.(SFKA,DELKA)-
                WRITEOUTPUT.2-
                E1=COS.(PI12)-.1.SIN.(PI12)-
                E2=COS.(P16)+.1.SIN.(P16)-
                DOTHROUGH(S100),I=1.1.I.LE.NKA-
                F1=1-I-
                FKA=SFKA+F1*DELKA-
                A=FKA/TP-
                F1=FLPFL.(A,R13)-
                DSQ=U1*F1*E1-
                F2=FLPFL.(FKA,R13)-
                X1=0.750*PI-
                F3=FLPFL.(X1,R23)-
                ALPH=F2*F3*E2/(4.*A)-
                X3=2.*FKA-
                E3=COS.(X3)-.1.SIN.(X3)-
                FL=PI*A-
                FLK=PI*FKA-
                E4=COS.(FLK)-.1.SIN.(FLK)-
                X5=-FL*ALPH +.1.0.-
                E5=CEXPL.(X5)-
                ECW=DSQ*E3*E4*E5-
                ECWT=2.*ECW-
                FAM=A*RATIO-
                EGO=0.5*FAM-
                EPO=EGO+.1.0.-
                ETOT=-EPO-ECWT-
                Y1=.REAL.ETOT-
                Y2=.IMAG.ETOT-
                FETSQ=(Y1*Y1)+(Y2*Y2)-
                SIGMA=4.*FETSQ/(A*A)-
                SIGMAW=2.*TP*FETSQ-
                SIGLOG=LOG.(SIGMAW)-
```

```
                Y3=.REAL.ECWT-
                Y4=.IMAG.ECWT-
                FMECW=SQRT.(Y3*Y3+Y4*Y4)-
                PHECW=FATAN2.(Y4,Y3)-
                PHDEC=RADEG*PHECW-
                WRITEOUTPUT,2,(FKA,SIGMA,EPO,ETOT,FMECW,PHDEC)-
                WRITEOUTPUT,2-
                   WRITEOUTPUT,2,(FKA,SIGMAW,SIGLOG)-
                WRITEOUTPUT,2-
    S100        CONTINUE-


                CALLSUBROUTINE()=ENDJOB.()-
                ENDPROGRAM(START)-
   ***          DATA
  00500
  0.1       0.1


  ***           RUN
  ***            DUMP LOWER CORE
  ***           SCATRAN
C    BACKSCATTER FROM A PROLATE SPHEROID USING GEOMETRICAL OPTICS AND
                CREEPING WAVE ANALYSIS -
C               FA = SEMI MAJOR AXIS -
C               FB = SEMI MINOR AXIS -
C               THT = ANGLE FROM MAJOR AXIS -
C               WAVE = WAVELENGTH -
                COMPLEX(ALPHL,GAMMAL,AECW,PL1,PL2,PHS,DSQ,ECW,ETOT)-
                COMPLEX(E1,E2,E3)-
                COMPLEX(CEXPL.)-
                COMPLEX(CGO,EGOC)-
                COMPLEX(EPO)-
C               COMPUTE LIST OF CONSTANTS -
   START        PI=3.1415927-
                TP=2.*PI-
                PI2=PI/2.-
                U1=0.270-
                U2=0.210-
                U2S=0.450-
                DELU2=0.050-
                NU2=3-
                R13=1./3.-
                R23=2./3.-
                R32=3./2.-
                PI4=PI/4.-
                PI34=3.*PI4-
                PI6=PI/6.-
                PI12=PI/12.-
                RADEG=57.29578-
                DEGRAD=0.01745329-
                E1=COS.(PI12)-.I.SIN.(PI12)-
                E2=COS.(PI6)+.I.SIN.(PI6)-
                E3=COS.(PI34)+.I.SIN.(PI34)-
                FEX=-0.5-
                FEXK= 0.5-
                READ INPUT,7,(FA,FB,THTS,DTHT)-
                WRITE OUTPUT,2,(FA,FB,THTS,DTHT)-
                READ INPUT,8, (NTHT,NWAVE)-
                WRITEOUTPUT,3,(NTHT,NWAVE)-
                WRITE OUTPUT,2-
                FAB=FA*FB-
                G3=FLPFL.(FAB,R23)-
                DOTHROUGH(S100),I=1,1.I.LE.NWAVE -
                READ INPUT,7,(WAVE)-
                FK=TP/WAVE -
                G1=FLPFL.(WAVE,R23)-
                G2=FLPFL.(WAVE,R13)-
                FKA=FK*FA-
```

```
            WRITE OUTPUT,FMT1,(WAVE) -
F FMT1      (5X,Q* WAVELENGTH = *,F15.8)-
            WRITE OUTPUT,FMT5,(FKA)-
F FMT5      (5X,Q*FKA = *,F10.5)-
            DO THROUGH(S100),KK=1,1,KK.LE.NU2-
            FKK=KK-
            U2=U2S+FKK*DELU2-
            WRITE OUTPUT,FMT3,(U2)-
F FMT3      (5X,Q* U2= *,F10.5)     -
            WRITE OUTPUT,FMT2-
F FMT2      (120H        THT            REECW            1MECW            REEGO
                      1MEGO            RETOT            IMETOT           SIGMA
                 )-
C           COMPUTE THE COMPLEX ATTENUATION CONSTANT OF THE CREEPING
            WAVE USING THE ELLIPTIC INTEGRAL -
            TCW1=PI2-
            TCW2=3.*PI2-
            CALL SUBROUTINE(PALPH)=FINCP.(TCW1,TCW2,0.01,2,FA,FB,FEX) -
            ALPHL=U2*E2*PALPH*G3/G2-
C           COMPUTE THE PATH LENGTH USING THE ELLIPTIC INTEGRAL -
            CALLSUBROUTINE(PALPHK)=FINCP.(TCW1,TCW2,0.01,2,FA,FB,FEXK)-
            FKTL=FK*PALPHK-
            GAMMAL=-ALPHL-.1.FKTL -
            AECW=CEXPL.(GAMMAL) -
            DO THROUGH(S10),J=1,1,J.LE.NTHT -
            FJ=J -
            THT=THTS+FJ*DTHT -
            RTHT=DEGRAD*THT -
C           COMPUTE POINTS OF ATTACHMENT AND DEPARTURE OF THE CREEPING
            WAVE -
            CS1=COS.(RTHT) -
            SS1=SIN.(RTHT) -
            CS2=CS1*CS1 -
            SS2=SS1*SS1 -
            XP=FA*FA*SS1/SQRT.(FA*FA*SS2+FB*FB*CS2)-
            XP=.ABS.XP-
            XM=-XP -
            YSQ=FB*FB*(1.-(XP*XP/(FA*FA))) -
            YP=SQRT.(YSQ) -
            YM=-YP -
            ANG1=FATAN2.(YP,XP) -
            TCW1=PI-ANG1-
            TCW2=PI+TCW1 -
C           COMPUTE THE CREEPING WAVE , GEOMETRICAL OPTICS, AND TOTAL
            BACKSCATTERED FIELDS -
            FR=SQRT.(XP*XP+YP*YP)-
            S1=FR*SIN.(TCW1-PI2-RTHT)-
            S2=S1 -
            FKS1=FK*S1-
            FKS2=FK*S2-
            PL1=1.+.1.0.-
            PL2=1.+.1.0.-
            PHS=PL1+PL2-
C           COMPUTE DSQ USING THE LOCAL RADIUS OF CURVATURE -
            COSL=COS.(ANG1)-
            SINL=SIN.(ANG1)-
            FRLA=FA*SINL-
            FRLB=FB*COSL-
            FRLP=FRLA*FRLA+FRLB*FRLB-
            FRL=(FLPFL.(FRLP.R32))/FAB-
            F1=FLPFL.(FRL.R13)-
            DSQ=U1*F1*G1*E1-
            ECW=-DSQ*AECW*PHS-
```

```
                XGO=FA*FA*CS1/SQRT.(FA*FA*CS2+FB*FB*SS2)-
                XGO=.ABS.XGO-
                YGO=FB*SQRT.(1.-XGO*XGO/(FA*FA))-
                YGO=.ABS.YGO-
                THTGO=FATAN2.(YGO.XGO)-
                FRGO=SQRT.(XGO*XGO+YGO*YGO)-
                RTGO=RTHT-THTGO-
                SGO=FRGO*COS.(RTGO)-
                SSGO=2.*FK*SGO-
                CGO=COS.(SSGO)+.1.SIN.(SSGO)-
                SRGO=FB*FB*SS2+FA*FA*CS2-
                 SQRGO=SQRT.(SRGO)-
                FACT=0.5*FB*FB*FA/SRGO-
                EPO=-FACT*(1.+.1.1./(2.*FK*SQRGO))-
                EGOC=EPO*CGO-

                ETOT=EGOC+ECW-
                EMAG1=.REAL.ETOT-
                EMAG2=.IMAG.ETOT-
                EMSQ=EMAG1*EMAG1+EMAG2*EMAG2-
                SIGMA=2.*TP*EMSQ/(WAVE*WAVE)-
                WRITEOUTPUT.2.(THT.ECW.EGOC.ETOT.SIGMA)-
                WRITE OUTPUT.FMT4.(S1)-
F FMT4          (5X.Q* S1 = *.F10.5)-
                ECW1=.REAL.ECW-
                ECW2=.IMAG.ECW-
                FMECW=SQRT.(ECW1*ECW1+ECW2*ECW2)-
                EGO1=.REAL.EGOC-
                EGO2=.IMAG.EGOC-
                FMEGO=SQRT.(EGO1*EGO1+EGO2*EGO2)-
                WRITEOUTPUT.2.(FMECW.FMEGO)-
                SIGMAL=LOG.(SIGMA)-
                SIGMAL=10.*SIGMAL-
                WRITE OUTPUT.FMT6.(SIGMAL)-
F FMT6          (5X.Q*SIGMAL= *.F10.5)-
                WRITE OUTPUT.2-
  S10           CONTINUE-
  S100          CONTINUE-
                CALL SUBROUTINE()=ENDJOB.()-
                 SUBROUTINE(SSS)=FINCP.(FLL.FUL.ERRR.NX.FMA.FMB.FEX)-
                FN=NX-
                DEL=(FUL-FLL)/FN-
                SSS=0.-
                ERR=0.01*ERRR/FN-
                A=FLL-
                DOTHROUGH(S40).NNX=1.1.NNX.LE.NX-
                MXX=0-
                B=A+DEL-
                SS=0.-
                MX=2-
                DX=DEL/2.-
                LX=1-
                X=A-
                TRANSFERTO(S15)-
  S5            TRAZ=DX*SS-
                MX=1-
                LX=1-
                DX=DEL-
  S10           SS=0.-
                LX=LX+1-
                DX=0.5*DX-
                X=A+DX-
```

```
  S15         DOTHROUGH(S20),IX=1,1,IX.LE.MX-
              GSIN=FMA*SIN.(X)-
              GCOS=FMB*COS.(X)-
              GGSS=GSIN*GSIN+GCOS*GCOS-
              FSS=FLPFL.(GGSS,FEX)-
  S18         SS=SS+FSS-
  S20         X=X+2.*DX-
              PROVIDED(LX.E.1),TRANSFERTO(S5)-
              MX=2*MX-
  S21         TRAP=0.5*TRAZ+DX*SS-
              DIF=.ABS.(TRAP-TRAZ)-
              PROVIDED(DIF.GE.DIP),MXX=MXX+1-
              DIP=DIF-
  S22         SIMP=(4.*TRAP-TRAZ)/3.-
  S23         FNCP=(16.*SIMP-SIMZ)/15.-
  S24         ER=.ABS.(1.-FNCZ/FNCP)-
              TRAZ=TRAP-
              SIMZ=SIMP-


              FNCZ=FNCP-
  S25         PROVIDED(LX.L.4),TRANSFERTO(S10)-
  S26         PROVIDED(MXX.G.4),TRANSFERTO(S30)-
  S27         PROVIDED(ER.G.ERR),TRANSFER TO (S10)-
  S30         SSS=SSS+FNCP-
  S40         A=A+DEL-
  S50         CONTINUE-
              NORMAL EXIT -
              END SUBPROGRAM-
C  ***  ORDER OF DATA CARDS ***-
C  CARD 1 FORMAT,7,(FA,FB,THTS,DTHT) -
C  CARD 2 FORMAT,8,(NTHT,NWAVE) -
C   NEXT NWAVE CARDS  FORMAT,7,(WAVE) -
              END PROGRAM(START) -
 ***           DATA
  4.0         2.0        -2.0          2.0
0004600003
  4.18879
  3.59038
  3.14159
```

```
 ***          RUN
 ***           OUMP LOWER CORE
 ***          SCATRAN
C    BACKSCATTER FROM A PROLATE SPHEROID USING GEOMETRICAL OPTICS ANO
             CREEPING WAVE ANALYSIS -
C            E FIELO PARALLEL TO PLANE OF INCIDENCE-
C            FA = SEMI MAJOR AXIS -
C            FB = SEMI MINOR AXIS -
C            THT = ANGLE FROM MAJOR AXIS -
C            WAVE = WAVELENGTH -
             COMPLEX(ALPHL,GAMMAL,AECW,PL1,PL2,PHS,OSQ,ECW,ETOT)-
             COMPLEX(E1,E2,E3)-
             COMPLEX(CEXPL,)-
             COMPLEX(CGO,EGOC)-
             COMPLEX(EPO)-
C            COMPUTE LIST OF CONSTANTS -
  START      PI=3.1415927-
             TP=2.*PI-
             PI2=PI/2.-
             UI=0.270-
             R13=1./3.-
             R23=2./3.-
             R32=3./2.-
             PI4=PI/4.-
             PI34=3.*PI4-
             PI6=PI/6.-
             PI12=PI/12.-
             RADEG=57.29578-
             OEGRAO=0.01745329-
             E1=COS.(PI12)-.I.SIN.(PI12)-
             E2=COS.(PI6)+.I.SIN.(PI6)-
             E3=COS.(PI34)+.I.SIN.(PI34)-
             FEXK= 0.5-
             READ INPUT,7,(FA,FB,FKAS,DFKA)-
             WRITE OUTPUT,2,(FA,FB,FKAS,OFKA)-
             READ INPUT,8,(NKA)-
             WRITE OUTPUT,3,(NKA)-
             REAO INPUT,7,(THT)-
             WRITE OUTPUT,2,(THT)-
             WRITE OUTPUT,2-
             RTHT=DEGRAO*THT -
             FAB=FA*FB-
             G3=FLPFL.(FAB,R23)-
             DO THROUGH(S100),I=1,1,I.LE.NKA-
             FI=I-
             FKA=FKAS+(FI-1.)*DFKA-
             FK=FKA/FA-
             WAVE=TP/FK-
             G1=FLPFL.(WAVE,R23)-
             G2=FLPFL.(WAVE,R13)-
             FKA=FK*FA-
             WRITE OUTPUT,FMT1,(WAVE) -
F FMT1       (5X,Q* WAVELENGTH = *,F15.8)-
             WRITE OUTPUT,FMT5,(FKA)-
F FMT5       (5X,Q*FKA = *,F10.5)-
             WRITE OUTPUT,FMT2-
F FMT2       (120H        THT            REECW          IMECW          REEGO
                       IMEGO            RETOT          IMETOT         SIGMA
                  )-
```

```
C            COMPUTE THE COMPLEX ATTENUATION CONSTANT OF THE CREEPING
             WAVE USING THE ELLIPTIC INTEGRAL -
             TCW1=P12-
             TCW2=PI-
             CALLSUBROUTINE(PALPH)=FINTA.(TCW1.TCW2.5.00.2.FA.FB)-
               ALPHL=E2*PALPH/G2-
              ALPHL=2.*ALPHL    -
C            COMPUTE THE PATH LENGTH USING THE ELLIPTIC INTEGRAL -
             CALLSUBROUTINE(PALPHK)=FINCP.(TCW1.TCW2.1.00.2.FA.FB.FEXK)-
             PALPHK=2.*PALPHK-
             FKTL=FK*PALPHK-
             GAMMAL=-ALPHL-.1.FKTL -
             AECW=CEXPL.(GAMMAL) -
C            COMPUTE POINTS OF ATTACHMENT AND DEPARTURE OF THE CREEPING
             WAVE -
             CS1=COS.(RTHT) -
             SS1=SIN.(RTHT) -
             CS2=CS1*CS1 -
             SS2=SS1*SS1 -
             XP=FA*FA*SS1/SQRT.(FA*FA*SS2+FB*FB*CS2)-
             XP=.ABS.XP-
             XM=-XP -
             YSQ=FB*FB*(1.-(XP*XP/(FA*FA))) -
             YP=SQRT.(YSQ) -
             YM=-YP -
             ANG1=FATAN2.(YP.XP) -
             TCW1=PI-ANG1-
             TCW2=PI+TCW1 -
C            COMPUTE THE CREEPING WAVE . GEOMETRICAL OPTICS. AND TOTAL
             BACKSCATTERED FIELDS -
             FR=SQRT.(XP*XP+YP*YP)-
             S1=FR*SIN.(TCW1-P12-RTHT)-
             S2=S1 -
             FKS1=FK*S1-
             FKS2=FK*S2-
             PL1=1.+.1.0.-
             PL2=1.+.1.0.-
             PHS=PL1+PL2-
C            COMPUTE OSQ USING THE LOCAL RADIUS OF CURVATURE -
             COSL=COS.(ANG1)-
             SINL=SIN.(ANG1)-
             FRLA=FA*SINL-
             FRLB=FB*COSL-
             FRLP=FRLA*FRLA+FRLB*FRLB-
             FRL=(FLPFL.(FRLP.R32))/FAB-
             F1=FLPFL.(FRL.R13)-
             OSQ=U1*F1*G1*E1-
             ECW=-OSQ*AECW*PHS-
             XGO=FA*FA*CS1/SQRT.(FA*FA*CS2+FB*FB*SS2)-
             XGO=.ABS.XGO-
             YGO=FB*SQRT.(1.-XGO*XGO/(FA*FA))-
             YGO=.ABS.YGO-
             THTGO=FATAN2.(YGO.XGO)-
             FRGO=SQRT.(XGO*XGO+YGO*YGO)-
             RTGO=RTHT-THTGO-
             SGO=FRGO*COS.(RTGO)-
             SSGO=2.*FK*SGO-
             CGO=COS.(SSGO)+.1.SIN.(SSGO)-
             SRGO=FB*FB*SS2+FA*FA*CS2-
              SQRGO=SQRT.(SRGO)-
```

```
                FACT=0.5*FB*FB*FA/SRGO-
                EPO=-FACT*(1.+.1.1./(2.*FK*SQRGO))-
                EGOC=EPO*CGO-
                ETOT=EGOC+ECW-
                EMAG1=.REAL.ETOT-
                EMAG2=.IMAG.ETOT-
                EMSQ=EMAG1*EMAG1+EMAG2*EMAG2-
                SIGMA=2.*TP*EMSQ/(WAVE*WAVE)-
                WRITEOUTPUT.2.(THT.ECW.EGOC.ETOT.SIGMA)-

                WRITE OUTPUT.FMT4.(S1)-
F FMT4          (5X.Q* S1 = *.F10.5)-
                ECW1=.REAL.ECW-
                ECW2=.IMAG.ECW-
                FMECW=SQRT.(ECW1*ECW1+ECW2*ECW2)-
                EGO1=.REAL.EGOC-
                EGO2=.IMAG.EGOC-
                FMEGO=SQRT.(EGO1*EGO1+EGO2*EGO2)-
                SIGMAL=LOG.(SIGMA)-
                SIGMAL=10.*SIGMAL-
                WRITE OUTPUT.FMT6.(SIGMAL.FMECW.FMEGO)-
F FMT6          (5X.Q*SIGMAL= *.F10.5.2X.Q*FMECW= *.F15.7.2X.Q*FMEGO= *.F15.
                7)-
                WRITE OUTPUT.2-
  S10           CONTINUE-
  S100          CONTINUE-
                CALL SUBROUTINE()=ENDJOB.()-
                SUBROUTINE(SSS)=FINTA.(FLL.FUL.ERRR.NX.FMA.FMB)-
                P1=3.1415927-
                R23=2./3.-
                FN=NX-
                DEL=(FUL-FLL)/FN-
                SSS=0.-
                ERR=0.01*ERRR/FN-
                A=FLL-
                DOTHROUGH(S40).NNX=1.1.NNX.LE.NX-
                MXX=0-
                B=A+DEL-
                SS=0.-
                MX=2-
                DX=DEL/2.-
                LX=1-
                X=A-
                TRANSFERTO(S15)-
  S5            TRAZ=DX*SS-
                MX=1-
                LX=1-
                DX=DEL-
  S10           SS=0.-
                LX=LX+1-
                DX=0.5*DX-
                X=A+DX-
  S15           DOTHROUGH(S20).IX=1.1.IX.LE.MX-
                SINX=SIN.(X)-
                COSX=COS.(X)-
                BSIN=FMB*SINX-
                BCOS=FMB*COSX-
                ASIN=FMA*SINX-
                ACOS=FMA*COSX-
                AACOS=.ABS.(ACOS)-
                FRE=SQRT.(ACOS*ACOS+BSIN*BSIN)-
                FRS2=ASIN*ASIN+BCOS*BCOS-
                FRS=SQRT.(FRS2)-
                FRP=FRS2*FRS/(FMA*FMB)-
                CPS1=-BCOS/FRS2-
```

```
            SIPSI=SQRT.(1.-CPSI*CPSI)-
            PSI=FATAN2.(SIPSI.CPSI)-
            PROVIDED(PSI.L.0.01).TRANSFER TO(S16)-
            AO=FRE*SIN.(P1-X)/SIN.(PSI)-
            AO=.ABS.(AO)-
            TRANSFER TO(S17)-
S16         AO=FMA-
S17         CONTINUE-
            DXE=AACOS-AO*COS.(PSI)-

            BO=FMB*SQRT.(1.-DXE*DXE/(FMA*FMA))-
            FRO=BO*BO/AO-
            RAT=FRP/FRO-
            XRAT=0.840*RAT-
            U2=0.20+(1.48/EXPE.(XRAT))-
            FARG=FLPFL.(FRP.R23)-
            FSS=U2*FRS/FARG-
S18         SS=SS+FSS-
S20         X=X+2.*DX-
            PROVIDED(LX.E.1).TRANSFERTO(S5)-
            MX=2*MX-
S21         TRAP=0.5*TRAZ+DX*SS-
            DIF=.ABS.(TRAP-TRAZ)-
            PROVIDED(DIF.GE.DIP).MXX=MXX+1-
            DIP=DIF-
S22         SIMP=(4.*TRAP-TRAZ)/3.-
S23         FNCP=(16.*SIMP-SIMZ)/15.-
S24         ER=.ABS.(1.-FNCZ/FNCP)-
            TRAZ=TRAP-
            SIMZ=SIMP-
            FNCZ=FNCP-
S25         PROVIDED(LX.L.4).TRANSFERTO(S10)-
S26         PROVIDED(MXX.G.4).TRANSFERTO(S30)-
S27         PROVIDED(ER.G.ERR).TRANSFER TO (S10)-
S30         SSS=SSS+FNCP-
S40         A=A+DEL-
S50         CONTINUE-
            NORMAL EXIT -
            END SUBPROGRAM-
             SUBROUTINE(SSS)=FINCP.(FLL.FUL.ERRR.NX.FMA.FMB.FEX)-
            FN=NX-
            DEL=(FUL-FLL)/FN-
            SSS=0.-
            ERR=0.01*ERRR/FN-
            A=FLL-
            DOTHROUGH(S40).NNX=1.1.NNX.LE.NX-
            MXX=0-
            B=A+DEL-
            SS=0.-
            MX=2-
            DX=DEL/2.-
            LX=1-
            X=A-
            TRANSFERTO(S15)-
S5          TRAZ=DX*SS-
            MX=1-
            LX=1-
            DX=DEL-
S10         SS=0.-
            LX=LX+1-
            DX=0.5*DX-
            X=A+DX-
```

```
S15         DOTHROUGH(S20),IX=1,1,IX.LE.MX-
            GSIN=FMA*SIN.(X)-
            GCOS=FMB*COS.(X)-
            GGSS=GSIN*GSIN+GCOS*GCOS-
            FSS=FLPFL.(GGSS,FEX)-
S18         SS=SS+FSS-
S20         X=X+2.*DX-
            PROVIDED(LX.E.1),TRANSFERTO(S5)-
            MX=2*MX-
S21         TRAP=0.5*TRAZ+DX*SS-
            DIF=.ABS.(TRAP-TRAZ)-
            PROVIDED(DIF.GE.DIP),MXX=MXX+1-
            DIP=DIF-
S22         SIMP=(4.*TRAP-TRAZ)/3.-
S23         FNCP=(16.*SIMP-SIMZ)/15.-
S24         ER=.ABS.(1.-FNCZ/FNCP)-
            TRAZ=TRAP-
            SIMZ=SIMP-
            FNCZ=FNCP-
S25         PROVIDED(LX.L.4),TRANSFERTO(S10)-
S26         PROVIDED(MXX.G.4),TRANSFERTO(S30)-
S27         PROVIDED(ER.G.ERR),TRANSFER TO (S10)-
S30         SSS=SSS+FNCP-
S40         A=A+DEL-
S50         CONTINUE-
            NORMAL EXIT -
            END SUBPROGRAM-
C   ***  ORDER OF DATA CARDS ***-
C            DATA CARD 1 FORMAT,7,(FA,FB,FKAS,DFKA)-
C            DATA CARD 2 FORMAT,8,(NKA)-
C            DATA CARD 3 FORMAT,7,(THT)-
            END PROGRAM(START) -
 ***         DATA
  2.0       1.0        0.5         0.1
00100
  90.
```

REFERENCES

1. Peters, L., Jr., "The End Fire Echo Area of Long Thin Bodies," IRE Transactions on Antennas and Propagation, Vol. AP-6, No. 1, (January 1958).

2. Senior, T.B.A., "A Survey of Analytical Techniques for Cross-Section Estimation," Proc. IEEE, Vol. 53, No. 8, (August 1965), pp. 822-833.

3. Franz, W., and Depperman, K., "Theorie der Beugang Am Zylinder unter Berücksichtigung der Kreichwelle," Ann. Physik, Vol. 10, (June 1952), pp. 361-373.

4. Keller, J.B., and Levy, B.R., "Diffraction by a Smooth Object," New York University Research Report EM 109.

5. Keller, J.B., and Levy, B.R., "Decay Exponents and Diffraction Coefficients for Surface Waves or Surfaces on Non-Constant Curvature," Symposium on Electromagnetic Theory, Professional Group on Antennas and Propagation, Institute of Radio Engineers, (December 1959), pp. 552-561.

6. Voltmer, David R., Ph.D. Dissertation to be published. The Ohio State University, Columbus, Ohio.

7. Cohen, J.H., "The Echo Area of an Ogive with Various Terminations," Report 1815-3, 1 June 1965, Antenna Laboratory, The Ohio State University Research Foundation; prepared under Subcontract No. 28-5041, Lockheed Missiles and Space Company, A Group Division of Lockheed Aircraft Corporation, Sunnyvale, California.

8. Moreland, J.P., L. Peters, Jr., and T.E. Kilcoyne, "Further Studies of Echo Area Contributions of Creeping Waves," Report 1815-5, 31 July 1965, Antenna Laboratory, The Ohio State University Research Foundation; prepared under Subcontract No. 28-5041, Lockheed Missiles and Space Company, A Group Division of Lockheed Aircraft Corporation, Sunnyvale, California.

9. Moffatt, D.L., "Low Radar Cross Sections, The Cone-Sphere," Report 1223-5, 15 May 1962, Antenna Laboratory, The Ohio State University Research Foundation; prepared under Contract No.

AF 33(616)-8039, Aeronautical Systems Division, Wright-Patterson Air Force Base, Ohio. (AD 283 338).

10. Bechtel, M.E., "Application of Geometric Diffraction Theory to Scattering from Cones and Disks," Proc. IEEE, Vol. 53, No. 8, (August 1965), p. 877.

11. Peters, L. Jr., "Modifications of Geometrical Theory of Diffraction for Non-Cylindrical Curved Surfaces," Report 1815-2, 5 March 1965, Antenna Laboratory, The Ohio State University Research Foundation; prepared under Subcontract No. 28-5041, Lockheed Missiles and Space Company, A Group Division of Lockheed Aircraft Corporation, Sunnyvale, California.

12. Moffatt, D.L., "Electromagnetic Scattering by a Perfectly Conducting Prolate Spheroid," Report 1774-11, 10 September 1965, Antenna Laboratory, The Ohio State University Research Foundation; prepared under Contract AF 33(615)-1318, Research and Technology Division, Wright-Patterson Air Force Base, Ohio. (AD 476 246).

13. Franz, W., and Depperman, K., "Theorie der Beugang der Kugel unter Berücksichtigung der Kreichwelle, Ann. Physik, Vol. 14, (June 1954), pp. 253-264.

14. Senior, T.B.A., and Goodrich, R.F., "Scattering by a Sphere," Proc. IEE, Vol. 111, No. 5, (May 1964).

15. Kouyoumjian, R.G., Unpublished Notes on Electromagnetic Theory. (In preparation for a book).

16. Keller, op. cit., Ref. 4.

17. Seigel, K.M., et. al., "Studies in Radar Cross-Sections - VIII," Willow Run Research Center, Engineering Research Institute - University of Michigan, Proj. MX-794 USAF Contract W33-038-ac-14222 UMM-115, (October 1953).

18. Pauli, W., "On Asymptotic Series for Functions in the Theory of Diffraction of Light," Physical Review, 54, (1 December 1938).

19. Blore, W.E., "The Radar Cross Section of Ogives, Double-Backed Cones, Double-Rounded Cones, and Cone Spheres," IEEE Trans. on Antennas and Propagation, Vol. AP-12, No. 5, (September 1964), p. 582.

20. Ufimtsev, P.Ia., "Approximate Calculation of the Diffraction of Plane Electromagnetic Waves by Certain Metal Objects II, The Diffraction by a Disc and by a Finite Cylinder," Zh. Tekh. Fiz. (USSR), Vol. 28, No. 11. (CC Trans) (1958) pp. 2604-16.

21. DeVore, R.V., and R.G. Kouyoumjian, "The Backscattering from a Circular Disc," URSI-IRE Spring Meeting, Washington, D.C., (May 1691).

22. Ryan, C.E., Jr., and R.C. Rudduck, "Calculation of the Radiation Pattern of a General Parallel-Plate Waveguide Aperture for the TEM and TE_{01} Waveguide Modes," Report 1693-4, 10 September 1964, Antenna Laboratory, The Ohio State University Research Foundation; prepared under Contract N62269-2184, U.S. Naval Air Development Center, Johnsville, Pennsylvania.

23. Ryan, C.E., Jr., and R.C. Rudduck, "Calculation of the Far Field Patterns of a Rectangular Waveguide," Report 1693-7, 20 November 1964, Antenna Laboratory, The Ohio State University Research Foundation; prepared under Contract N62269-2184, U.S. Naval Air Development Center, Johnsville, Pennsylvania. (AD 462 764)

24. Interim Engineering Report, Report 1423-6, 1 July 1963, Antenna Laboratory, The Ohio State University Research Foundation; prepared under Contract AF 30(602)-2711, Rome Air Development Center, Griffiss Air Force Base, New York. (RADC-TDR-63-391). (AD 419 496)

25. Oberhettinger, F., "On Asymptotic Series for Functions in the Theory of Diffraction of Waves by Wedges," Jour. Math. and Phys., 34, (1955), pp. 245-255.

26. Keller, J.B., "Diffraction by an Aperture," Journal of Applied Physics," 28, 4, (April 1957), pp. 426-444.

UNCLASSIFIED

Security Classification

DOCUMENT CONTROL DATA - R & D

(Security classification of title, body of abstract and indexing annotation must be entered when the overall report is classified)

1. ORIGINATING ACTIVITY *(Corporate author)*
The Ohio State University, ElectroScience Laboratory
Department of Electrical Engineering
1320 Kinnear Road, Columbus, Ohio

2a. REPORT SECURITY CLASSIFICATION
Unclassified

2b. GROUP
N/A

3. REPORT TITLE
MEMORANDUM ON ANALYSIS OF ECHO AREA OF TARGETS USING GEOMETRICAL THEORY OF DIFFRACTION AND CREEPING WAVE THEORY - 2430-1

4. DESCRIPTIVE NOTES *(Type of report and inclusive dates)*
None

5. AUTHOR(S) *(First name, middle initial, last name)*
Ryan, C. E., Jr.

6. REPORT DATE	7a. TOTAL NO. OF PAGES	7b. NO. OF REFS
July 1967	72	26

8a. CONTRACT OR GRANT NO.	9a. ORIGINATOR'S REPORT NUMBER(S)
AF 19(628)-67-C-0308	
b. PROJECT NO.	ESD-TR-67-519
c.	9b. OTHER REPORT NO(S) *(Any other numbers that may be assigned this report)*
d.	

10. DISTRIBUTION STATEMENT

11. SUPPLEMENTARY NOTES	12. SPONSORING MILITARY ACTIVITY
	Electronic Systems Division, Air Force Systems Command, United States Air Force, L G Hanscom Field, Bedford, Mass. 01730

13. ABSTRACT

A combination of creeping-wave analysis and diffraction theory has been developed for determining the radar cross section of bodies for which exact solutions are not available. The known solutions for the perfectly conducting cylinder and sphere have been used to specify attenuation and diffraction coefficients for the creeping wave. The creeping wave contribution is added to the geometrical optics or physical optics contribution from the specular point to determine the total scattered field. It is demonstrated that this type of solution is applicable to ogives, ogives with spherical caps, and prolate spheroids. Wedge diffraction theory has been combined with creeping wave analysis to calculate the edge-on backscatter of circular and ogival disks. It is necessary to modify the magnitudes, but not the forms, of the creeping wave attenuation and diffraction coefficients when treating a creeping wave on an edge. This form of analysis is adaptable to calculation of the radar cross section of composite bodies where both volumetric shapes and edges may occur in combination. Once the specular points, wedge diffraction points, and the attachment points and paths of the creeping waves are determined the computation of the scattered field is straightforward.

DD FORM 1 NOV 65 1473

UNCLASSIFIED

Security Classification

14. KEY WORDS	LINK A		LINK B		LINK C	
	ROLE	WT	ROLE	WT	ROLE	WT
radar cross section						
backscatter						
electromagnetic theory						
wedge diffraction						
creeping wave						
sphere						
prolate spheroid						
ogive						
circular disk						
ogival disk						
attenuation coefficient						
diffraction coefficient						
geometrical optics						
physical optics						